URLLC-Enabled Full-Duplex Cell-Free Massive MIMO Systems With Mobility

SRAVANI KURMA [1] **(Graduate Student Member, IEEE), KESHAV SINGH** [1] **(Member, IEEE),**
PRABHAT KUMAR SHARMA [2] **(Senior Member, IEEE), CHIH-PENG LI** [1] **(Fellow, IEEE),**
AND THEODOROS A. TSIFTSIS [3,4] **(Senior Member, IEEE)**

[1]Institute of Communications Engineering, National Sun Yat-sen University, Kaohsiung 80424, Taiwan

[2]Department of Electronics and Communication Engineering, Visvesvaraya National Institute of Technology, Nagpur 440010, India

[3]Department of Informatics and Telecommunications, University of Thessaly, 35100 Lamia, Greece

[4]Department of Research and Development, InnoCube P.C., 55535 Thessaloniki, Greece

CORRESPONDING AUTHOR: C.-P. LI (e-mail: cpli@faculty.nsysu.edu.tw)

ABSTRACT In the rapidly evolving domain of intelligent vehicular systems, reliable and instantaneous communication is paramount. This paper delves into the robustness of an ultra-reliable low-latency communication (URLLC)-enabled full-duplex cell-free massive multiple-input multiple-output (FD-CFm-MIMO) system, considering the unique challenges presented by mobile vehicular networks. Recognizing the constraints of real-world fronthaul links, we focus on a uniform fronthaul quantization strategy. Our primary contribution is deriving the cumulative distribution function (CDF) of the signal-to-interference-plus-noise ratio (SINR) at each receiver. We utilize the Welch-Satterthwaite approximation, taking into account the effects of imperfect channel state information (CSI) and the inherent mobility of vehicle communication units (VCUs). Building upon this, we present closed-form expressions of outage probability for both infinite and finite block-length transmission models. A comparative study using Monte Carlo simulations validates our analytical derivations. We consider the half-duplex CFm-MIMO system as a benchmark scheme. Our results underscore the significant influence of several system parameters, such as transmit power, VCU mobility, CSI accuracy, fronthaul link quality, residual interference (RI), and quantization nuances, Doppler power spectra models, pilot contamination on overall system performance.

INDEX TERMS Outage probability, cell-free massive multiple-input and multiple-output (CFm-MIMO), confined fronthaul link, ultra-reliable low latency communication (URLLC), vehicle communication, mobility.

I. INTRODUCTION

ULTRA-RELIABLE low-latency communication (URLLC) has emerged as a pivotal component in the transition from 5G to more advanced networking paradigms [1], [2]. It caters not only to the broader IoT sphere, such as industrial automation and public safety but, most crucially, to intelligent vehicular systems [3].

These advanced vehicular networks demand impeccable communications for their safe, efficient, and autonomous operations. With the burgeoning development of autonomous and connected vehicles, the need for URLLC becomes even more pronounced, where every microsecond could be the thin line between operational success and catastrophic failures on roads [4]. This underscores the need to dive deeper into

specific vehicular applications, particularly those that operate at consistent speeds [1], [5] namely, autonomous vehicles, public transportation, emergency services, Industrial IoT and so on.

Consistent speed vehicular applications are central to the broader vision of intelligent transportation [5], [6], [7]. For instance, automated convoys of trucks navigating highways, maintaining consistent speeds to optimize traffic flow and fuel efficiency or consider autonomous drones coordinating flawlessly in airspaces for tasks ranging from package deliveries to infrastructure monitoring. These aren't just futuristic scenarios; they represent the very heart of next-gen transportation, underscoring the unmatched value of predictability, precision, and synchronized operations. While high-speed vehicular networks battle with rapid channel variations, vehicles operating at consistent speeds face a unique set of challenges [6]. One of the primary challenges is ensuring seamless real-time responsiveness in their operations [3]. Even a slight delay or jitter in communication can disrupt synchronized tasks, such as precise inventory movement or infrastructure surveillance, potentially jeopardizing the system's efficiency and safety. To combat this challenge, URLLC is incorporated, ensuring that communication is not only swift but also reliable, mitigating the risks associated with latency issues [1], [2].

To effectively serve these smart transportation systems, it's not enough to merely rely on URLLC [3]. The integration of URLLC with cutting-edge 6G innovations, like cell-free massive MIMO (CFm-MIMO), becomes indispensable. CFm-MIMO combines the advantages of massive MIMO with a decentralized approach, resolving challenges related to inter-cell handovers, shadowing, and signaling interference, which are particularly significant in mobile vehicular contexts [8], [9]. However, the very essence of CFm-MIMO poses an intrinsic predicament: the need to exchange vast amounts of data between multiple APs and the central processing unit (CPU), often resulting in overwhelming bandwidth demands and increased latency on the fronthaul links. Implementing a confined fronthaul with uniform quantization becomes the solution, as it efficiently manages bandwidth by representing continuous signals with a finite number of levels, thus optimizing data traffic and reducing latency.

Other important challenge of intelligent vehicles is their dynamic movement which occurs due to the rapid changes in channel conditions. Herein lies the importance of the Doppler power spectra (DPS) models [10], [11], [12]. These models, grounded in the doppler effect, capture the frequency shifts due to vehicular speed and direction. By employing DPS models, communication systems can better predict, and thus mitigate the adverse impacts of vehicular mobility on communication links, ensuring more stable and reliable connections. In addition, imperfect channel state information (CSI) further complicates the task of maintaining reliable communication in the context of dynamic VCU movement [10]. Imperfect CSI can arise from inaccuracies in estimating channel conditions due to factors like signal blockage, multipath propagation, and

environmental changes. Inaccurate CSI can lead to suboptimal beamforming, increased interference, and reduced overall system performance. Addressing imperfect CSI becomes crucial to overcome these challenges. By combining DPS models and addressing imperfect CSI, communication systems achieve a higher level of adaptability. Accurate doppler modeling assists in predicting how VCU movement affects communication channels while addressing imperfect CSI mitigates the negative impact of estimation errors. Together, these approaches empower intelligent vehicles to maintain consistent, high-quality communication even in dynamic scenarios, contributing to safer and more efficient vehicular networks.

Few other important challenges in intelligent vehicles include real-time communication, safety coordination, and data-intensive operations [13], [14]. In this bustling matrix, full-duplex communication stands as a monumental breakthrough. It addresses these challenges by enabling instant interaction, enhancing safety through rapid data exchange, facilitating efficient coordination among vehicles, and supporting seamless transmission of sensor data for improved decision-making [14], [15]. Unlike half-duplex systems where transmission and reception happen in alternating times or frequencies, full-duplex systems enable simultaneous transmission and reception on the same frequency channel. This essentially doubles the spectral efficiency—a paramount advantage in vehicular networks where communication latency can be the difference between safe transit and mishaps [14]. Moreover, full-duplex communication paves the way for real-time adaptive responses, essential for autonomous driving scenarios, and vehicle-to-everything (V2X) interactions [14].

A. BACKGROUND WORKS AND MOTIVATION

Recent research on CFm-MIMO is expansive [2], [8], [9], [16], [17], [18], [19], [20]. While, the authors in [2] investigated the throughput analysis and characterization of the packet error probability for the half-duplex (HD) CFm-MIMO system under the URLLC regime, the study in [8] demonstrated significant throughput improvements and enhanced immunity to spatial fading, outperforming traditional small-cell approaches. A recent advancement has been integrating CFm-MIMO and full-duplex (FD), where access points (APs) serve uplink (UL) VCUs and downlink (DL) VCUs simultaneously on the same spectrum resource [16]. Assuming confined fronthaul, the works [16] and [17] have considered HD-CFm-MIMO and FD-CFm-MIMO systems, respectively.

While resource allocation and optimization of the spectrum, and energy efficiency have been the focus of all the works previously mentioned, this analysis neglected to take another critical performance metric into account, i.e., outage probability (OP). It is worth acknowledging that it is rather difficult to determine the formulation of the OP in closed-form expression [18]. Over rayleigh fading channels, AP is assumed to have imperfect channel state information (CSI), which leads

to the approximation of the OP for UL CFm-MIMO [19]. However, the analysis of the VCU mobility and fronthaul quantization is still missing in this study.

The authors in [21] investigate UL signal detection in limited-fronthaul, highly correlated channel conditions within scalable CF-mMIMO systems. It introduces two robust receivers that leverage effective noise heteroscedastic covariance to enhance performance. Additionally, the paper examines antenna distribution optimization in this context. While the authors in [14] focused on optimizing FD considering VCU mobility and without accounting for imperfect CSI, the authors in [10], [11] have examined the outage performance of FD systems considering VCU mobility and imperfect CSI from a practical standpoint under cellular architectures. Some prior works [20], [22], [23], [24] have explored the mobility aspect in CFm-MIMO systems. The authors in [22] investigated the impact of changing serving AP sets on scalable CF-mMIMO in mobile networks, deriving handover rates and analyzing mobility-aware throughput. The authors in [23] examined the interaction between cell-free massive MIMO systems at mmWave frequencies and VCU mobility, introducing a mmWave channel model considering channel aging, and presenting three beamforming techniques along with dynamic VCU association. The authors in [24] have investigated the spectral efficiency performance of CFm-MIMO-orthogonal frequency-division multiplexing systems in high-speed train (HST) communications, considering Doppler frequency offset and various combining techniques. The outage performance analysis of UL CFm-MIMO system is examined in [20] considering VCU mobility. However, it is essential to underscore that none of the previously mentioned works [20], [21], [22], [23], [24] have delved into the analysis of URLLC or conducted comprehensive outage probability assessments, leaving a notable gap in our understanding of these critical aspects in the context of CFm-MIMO systems.

CFm-MIMO's integration with full-duplex (FD) techniques, enabling APs to serve both UL-VCUs and DL-VCUs concurrently, stands out. However, a glaring omission in much of the literature is a comprehensive examination of the outage probability (OP), especially given its crucial significance in vehicular networks where even a momentary communication lapse can be catastrophic. Vehicular communication introduces a unique set of challenges, such as rapidly changing channel conditions due to the mobility of vehicles, stringent ultra-reliable low latency communication (URLLC) demands, and the complexities of handling fronthaul quantization issues. While preliminary studies, including our previous work [12], introduced the topic, they often overlooked the intricate interplay between these challenges. To put our contribution in perspective, we present a detailed comparative study in Table 2, pitting the state-of-the-art against our groundbreaking research. Notably, the investigation of URLLC-enabled FD CFm-MIMO systems for intelligent vehicles while addressing the dynamic nature of VCU mobility and the imperfections in channel state

information (CSI) has been a conspicuous gap in the literature. Our study's primary focus on analyzing the impact of different Doppler power spectra (DPS) models on the outage probability (OP) not only pushes the boundaries of existing research but also provides a crucial foundation for addressing the multifaceted challenges posed by vehicular communication systems. By illuminating the intricate relationship between DPS models and system reliability in the context of URLLC, our work offers valuable insights that are particularly pertinent to ensuring seamless and reliable communication in intelligent transportation systems.

B. CONTRIBUTION

Motivated by the background works, our paper uniquely advances the exploration of URLLC in an FD-CFm-MIMO consistent speed vehicular network, taking into account VCU mobility, quantized fronthaul, and imperfect CSI, laying a foundation for the development of safer and more efficient intelligent vehicular systems. Our key contributions to our work are listed as follows

1) ENHANCED MODELING OF URLLC PARADIGM

- *Introduction of Time-Selective Fading and Channel Estimation Error (CEE):* Unlike existing studies such as [12], our research places a significant emphasis on the URLLC paradigm. We include a dedicated section on channel estimation considering time-selective fading, where we analyze the impact of the minimum-mean-squared-error (MMSE) estimation technique on system performance. We introduce time-selective fading and CEE to encapsulate VCU mobility and the imperfections in CSI.
- *Exploration of VCU Mobility Models:* We extend our investigation to explore VCU mobility with Rectangular, Uniform, and Gaussian DPS models, providing a comprehensive understanding of their impact on URLLC performance.

2) ANALYTICAL FRAMEWORK DEVELOPMENT

- *Derivation of Closed-Form Expression for OP:* We present the derivation of a closed-form expression for OP using the Welch-Satterthwaite approximation. This analytical framework is grounded in realistic assumptions tied to VCU mobility, quantized fronthaul with confined capacity, and imperfect CSI.
- *Asymptotic M and N Analysis:* Additionally, we conduct asymptotic M and N analysis to further characterize the system behavior under varying conditions. This analysis provides insights into the scalability and robustness of the proposed system architecture.

3) SYSTEM PERFORMANCE EVALUATION AND PARAMETER ANALYSIS

- *Benchmarking FD CFm-MIMO with HD CFm-MIMO:* We provide benchmark analysis by comparing the performance of FD CFm-MIMO with HD CFm-MIMO,

TABLE 1. Tabulated comparative overview: state-of-the-art vs. our contribution.

Paper	[2]	[8]	[12]	[15]	[17]	[18]	[19]	[20]	[22]	[25]	[26]	Our work
URLLC regime	X	X	X	X	X	X	X	X	X	X	X	✓
Transmission mode	HD	HD	FD	FD	FD	HD	HD	HD	HD	FD	FD	FD
$\mathcal{M}$-Analysis	X	✓	✓	✓	X	X	X	X	X	X	X	✓
Imperfect CSI	X	✓	✓	✓	X	X	✓	✓	X	✓	✓	✓
Mobility	X	✓	✓	X	X	X	X	✓	✓	X	X	✓
Asymptotic Analysis	X	X	✓	✓	X	X	X	X	X	✓	X	✓
RI	X	X	✓	✓	✓	X	X	X	X	X	✓	✓
IUI	X	✓	✓	✓	✓	✓	X	X	X	✓	✓	✓
UDI	X	X	✓	✓	✓	X	X	X	X	✓	✓	✓
Confined Fronthaul Link	X	X	✓	X	X	X	X	X	X	X	X	✓

offering insights into the trade-offs between these configurations.

- *Influence of Various Parameters:* Building upon the foundational insights, we scrutinize how various parameters such as DL power, VCU mobility, the nature of CSI, fronthaul link specifications, and the metrics of uniform quantization influence the system performance under the URLLC regime.

- *Effects of Pilot Contamination, Time-Selective Fading, and CEE:* Specifically, we delve into the effects of pilot contamination, time-selective fading, and CEE, providing a comprehensive understanding of their implications on URLLC in the context of vehicular networks.

II. SYSTEM AND CHANNEL MODELS

We consider a URLLC-enabled FD-CFm-MIMO system that comprises geographically dispersed M APs and randomly distributed K_u UL and K_d DL VCUs. Each AP has N_r receive and N_t transmit antennas, whereas each VCU is equipped with a single antenna. A confined fronthaul link is used to connect every AP to the central processing unit (CPU) and thus jointly serves K (i.e., $K = (K_u + K_d)$) HD-VCUs.

A. CHANNEL DESCRIPTION

Let $\mathbf{g}_{mk}^d \in \mathbb{C}^{N_t \times 1}$ denotes the channel gain between the mth AP and k^{th} DL-VCU while $\mathbf{g}_{ml}^u \in \mathbb{C}^{N_r \times 1}$ represents the channel gain between the mth AP and l^{th} UL-VCU. These channels are modeled as $\mathbf{g}_{ml}^u = (\beta_{ml}^u)^{1/2} \tilde{\mathbf{g}}_{ml}^u$ and $\mathbf{g}_{mk}^d = (\beta_{mk}^d)^{1/2} \tilde{\mathbf{g}}_{mk}^d$. The distribution of co-channel interference (CCI) channel from the kth DL-VCU to the lth UL-VCU is given by $h_{kl} = (\tilde{\beta}_{kl})^{1/2} \tilde{h}_{kl}$ [8], [25]. Here, $\tilde{\beta}_{kl}$ is the large-scale fading coefficient that captures the signal attenuation due to path loss and shadowing effects between the kth and l^{th} VCU. The small-scale fading coefficients, such as $\tilde{h}_{kl}$, $\tilde{\mathbf{g}}_{mk}^d$, and $\tilde{\mathbf{g}}_{ml}^u$, are modeled as complex Gaussian random variables with a Rayleigh distribution, representing the rapid amplitude
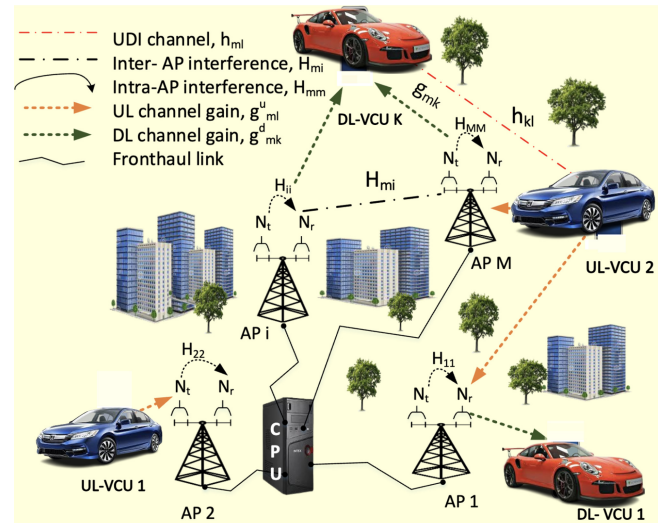

FIGURE 1. URLLC-enabled FD-CFm-MIMO system model.

fluctuations due to multipath propagation. These coefficients are independent and non-identically distributed (i.n.i.d.) with parameter σ_{mj}, where $j \in \{k, l\}$. Furthermore, $\mathbf{H}_{mi} \in \mathbb{C}^{N_r \times N_t}$, $1 \leq i \leq M$ represents the channel gain between the receive and transmit antennas of the mth and i^{th} AP, respectively. Accounting for shadow fading and path-loss, the large scale fading coefficient $\beta_{mj} \in \{\beta_{mk}^d, \beta_{ml}^u, \tilde{\beta}_{kl}\} \in \mathbb{R}$ is defined as

$$\beta_{mj} = PL_{mj}F_{mj}. \quad (1)$$

Here, the shadowing correlation factor is denoted by $F_{mj} = 10^{(\sigma_{th}z_{mj}/10)}$ with a log-normal standard deviation of σ_{th}, the independent and identically distributed (i.i.d) random variables $\{a_{mj}, b_{mj}\} \in \mathcal{N}(0, 1)$ follow a standard normal distribution, which characterizes VCU shadow fading effect, PL_{mj} denotes path-loss [12], and $z_{mj} = \sqrt{\delta}a_{mj} + \sqrt{1-\delta}b_{mj}$, where δ is the shadowing correlation coefficient.

B. CHANNEL ESTIMATION

The channel estimation process is conducted in accordance with the TDD protocol. Within the TDD frame, we distinguish three distinctive phases: the UL training phase, the UL data transmission phase, and the DL data transmission phase. This division of the TDD frame ensures an organized and efficient utilization of time resources for channel estimation and data transmission. Let τ represent the total number of samples within the coherence time interval T. We define τ_c as the number of samples in the UL training phase, which has a duration of T_c. Here, τ_u and τ_d represent the number of samples during UL transmission and DL transmission, lasting for a duration of T_u and T_d, respectively. During the UL training phase, τ_c can be expressed as the sum of two components: $\tau_c = \tau_c^d + \tau_c^u$, where, τ_c^d and τ_c^u represent the number of samples utilized as pilots for the DL VCUs and UL VCUs, respectively.

To estimate the channel, all DL VCUs and UL VCUs simultaneously transmit pilot signals. In this phase, the antennas at each AP operate exclusively in receive mode, including both N_t and N_r antennas. The pilot sequences $\sqrt{\tau_c^d}\boldsymbol{\phi}_1^d \ldots \sqrt{\tau_c^d}\boldsymbol{\phi}_K^d$ and $\sqrt{\tau_c^u}\boldsymbol{\phi}_1^u \ldots \sqrt{\tau_c^u}\boldsymbol{\phi}_J^u$, sent by DL and UL VCUs respectively, are received by the antennas at the AP, obtaining channel estimates during the UL training phase. Here, $\boldsymbol{\phi}$ represents the pilots drawn from the set $\{\boldsymbol{\phi}_k^d, \boldsymbol{\phi}_j^u, \forall k, j\}$. The condition $|\boldsymbol{\phi}_k^d|^2 = 1$ applies to DL VCUs, while $|\boldsymbol{\phi}_j^u|^2 = 1$ is for UL VCUs [27]. The pilot signal received by the transmit and receive antennas of the mth AP can be respectively written as [16]

$$\mathbf{Y}_m^t = \sqrt{\tau_c^d \rho_t} \sum_{k=1}^{K} \mathbf{g}_{mk}^d \left(\boldsymbol{\phi}_k^d\right)^H + \mathbf{N}_m^t, \tag{2}$$

$$\mathbf{Y}_m^r = \sqrt{\tau_c^u \rho_t} \sum_{j=1}^{J} \mathbf{g}_{ml}^u \left(\boldsymbol{\phi}_l^u\right)^H + \mathbf{N}_m^r. \tag{3}$$

Here, ρ_t is the normalized pilot transmit power. $\mathbf{N}_m^t \in \mathbb{C}^{N_t \times \tau_c^d}$ and $\mathbf{N}_m^r \in \mathbb{C}^{N_r \times \tau_c^u}$ represent additive noise with $\mathcal{CN}(0, 1)$ entries. To minimize CSI exchange overhead, each AP estimates its channels with the UL and DL individually. To estimate the channels $\mathbf{g}_{mk}^d$ and $\mathbf{g}_{ml}^u$, the mth AP projects the received signal onto the pilot signals $\boldsymbol{\phi}_k^d$ and $\boldsymbol{\phi}_l^u$ respectively, as

$$\hat{\mathbf{y}}_{mk}^t = \mathbf{Y}_m^t \boldsymbol{\phi}_k^d = \sqrt{\tau_c^d \rho_t} \mathbf{g}_{mk}^d + \mathbf{N}_m^t \boldsymbol{\phi}_k^d, \tag{4}$$

$$\hat{\mathbf{y}}_{ml}^r = \mathbf{Y}_m^r \boldsymbol{\phi}_l^u = \sqrt{\tau_c^u \rho_t} \mathbf{g}_{ml}^u + \mathbf{N}_m^r \boldsymbol{\phi}_l^u. \tag{5}$$

These projections are used to compute the corresponding linear MMSE channel estimates [16] as

$$\hat{\mathbf{g}}_{mk}^d = \mathbb{E}\left\{\mathbf{g}_{mk}^d \left(\hat{\mathbf{y}}_{mk}^t\right)^H\right\} \left(\mathbb{E}\left\{\hat{\mathbf{y}}_{mk}^t \left(\hat{\mathbf{y}}_{mk}^t\right)^H\right\}\right)^{-1} \hat{\mathbf{y}}_{mk}^t$$
$$= c_{mk}\hat{\mathbf{y}}_{mk}^t, \tag{6}$$

$$\hat{\mathbf{g}}_{ml}^u = \mathbb{E}\left\{\mathbf{g}_{ml}^u \left(\hat{\mathbf{y}}_{ml}^r\right)^H\right\} \left(\mathbb{E}\left\{\hat{\mathbf{y}}_{ml}^r \left(\hat{\mathbf{y}}_{ml}^r\right)^H\right\}\right)^{-1} \hat{\mathbf{y}}_{ml}^r$$
$$= c_{ml}\hat{\mathbf{y}}_{ml}^r, \tag{7}$$

where $c_{mk} = \frac{\sqrt{\tau_c^d \rho_t}\beta_{\mathbf{g}_{mk}^d}}{\tau_c^d \rho_t \beta_{\mathbf{g}_{mk}^d} + 1}$ and $c_{ml} = \frac{\sqrt{\tau_c^u \rho_t}\beta_{\mathbf{g}_{ml}^u}}{\tau_c^u \rho_t \beta_{\mathbf{g}_{ml}^u} + 1}$.

The estimation error vectors[1] are defined as $\mathbf{g}_{\epsilon_{jm}}^u \triangleq \mathbf{g}_{ml}^u - \hat{\mathbf{g}}_{ml}^u$ and $\mathbf{g}_{\epsilon_{mk}}^d \triangleq \mathbf{g}_{mk}^d - \hat{\mathbf{g}}_{mk}^d$. With MMSE channel estimation, $\hat{\mathbf{g}}_{mk}^d$, $\mathbf{g}_{\epsilon_{mk}}^d$, $\hat{\mathbf{g}}_{ml}^u$, and $\mathbf{g}_{\epsilon_{jm}}^u$ are mutually independent and their individual terms are independent and identically distributed (i.i.d.) random variables with distribution $\mathcal{N}(0, \beta_{\hat{\mathbf{g}}_{mk}^d})$, $\mathcal{N}(0, \beta_{\mathbf{g}_{mk}^d} - \beta_{\hat{\mathbf{g}}_{mk}^d})$, $\mathcal{N}(0, \beta_{\hat{\mathbf{g}}_{ml}^u})$, and $\mathcal{N}(0, \beta_{\mathbf{g}_{ml}^u} - \beta_{\hat{\mathbf{g}}_{ml}^u})$, respectively, with $\beta_{\hat{\mathbf{g}}_{mk}^d} = \frac{\tau_c^d \rho_t (\beta_{\mathbf{g}_{mk}^d})^2}{\tau_c^d \rho_t \beta_{\mathbf{g}_{mk}^d} + 1}$ and $\beta_{\hat{\mathbf{g}}_{ml}^u} = \frac{\tau_c^u \rho_t (\beta_{\mathbf{g}_{ml}^u})^2}{\tau_c^u \rho_t \beta_{\mathbf{g}_{ml}^u} + 1}$.

After channel estimation, data transmission starts simultaneously for both DL and UL.

C. MOBILITY ANALYSIS

In this study, we have incorporated DPS models to analyze the dynamic nature of VCU mobility and its impact on the OP. The mobility of VCUs introduces time-selective i.n.i.d. block fading channels, which necessitate a robust model to accurately capture the channel variations over time [10]. To address this, we have employed the following DPS models, each with its practical implications:

- *Gaussian Model:* This model is particularly suited for environments with high relative speeds between the transmitter and receiver, such as in high-speed vehicular communications. It provides a comprehensive range of Doppler shifts, capturing the extensive variability in channel conditions due to rapid movement.
- *Uniform Model:* This model is applied in scenarios where Doppler shifts are expected to be uniformly distributed, such as in pedestrian or low-mobility settings. This model aids in the design of systems that can consistently handle the uniform distribution of frequency shifts across the specified range.
- *Rectangular Model:* This model assumes a constant DPS within a narrow frequency range, making it ideal for situations with limited and predictable mobility patterns, like indoor communication systems. It simplifies the analysis and mitigation of Doppler effects in such controlled environments.

Each model is associated with a specific formula ($S_C(f)$) that describes the distribution of frequency shifts due to the Doppler effect. The Table 2 compares various DPS models and their corresponding correlation coefficients. These models capture the frequency shifts caused by movement in wireless communication systems.

The correlation coefficients (φ) shed light on signal relationships affected by these models, aiding in understanding signal propagation and mitigation strategies. Moreover, to investigate the imperfect CSI along with the VCU's mobility,

---

[1] Note that the estimation error acts as an additional interference at each receiver. Therefore, it is a common notion in literature to consider it as Gaussian distributed [8], [16].

TABLE 2. Comparison of DPS models and their correlation coefficients [28].

Sr. No.	Type	DPS model, $S_C(f)$	Correlation Coefficient, φ
1	Gaussian	$\frac{S_0}{\sqrt{\pi}B_D} e^{\frac{-f^2}{B_D{}^2}}$	$e^{-(\pi B_D T)^2}$
2	Uniform	$\frac{S_0}{\pi\sqrt{B_D{}^2-f^2}}, |f| < 2B_D$	$J_0(2\pi B_D T)$
3	Rectangular	$\frac{S_0}{2B_D}, |f| < 2B_D$	$\text{sinc}(2B_D T)$

we represent the $\hat{\mathbf{g}}^o_{mj}$ at z^{th} signaling period in terms of its first signaling period $\hat{\mathbf{g}}^o_{mj}(1)$ and its mobility correlation parameter φ_{mj}, which is given as $\varphi_{mj} = \mathcal{J}0(\frac{2\pi f V_{mj}}{cR_s})$ [10], where V_{mj}, f, c, R_s denote relative speed, carrier frequency, symbol transmission rate and speed of light, respectively.

In the context of time-selective fading, the AP employs a pilot signal during the first signaling period of each transmission block to estimate the channel ($\mathbf{g}^o_{mj}$) at any given (z^{th}) signaling period. This estimation is crucial to adapt to the channel variations caused by the mobility of the VCUs. The estimated channel at the (z^{th}) signaling period is expressed as:

$$\hat{\mathbf{g}}^o_{mj}(z) = \beta^{1/2}_{mj}\left(\varphi^{z-1}_{mj}\hat{\mathbf{g}}^o_{mj}(1) + \boldsymbol{\Theta}^o_{mj}(z)\right), \qquad (8)$$

where $\boldsymbol{\Theta}^o_{mj}(z)$ represents the additive mobility noise. The term (φ^{z-1}_{mj}) accounts for the channel's correlation from the first to the (z^{th}) signaling period, reflecting the impact of VCU mobility on the channel's coherence over time. The additive mobility noise ($\boldsymbol{\Theta}^o_{mj}(z)$) captures the random variations in the channel, including the effects of noise and other uncertainties in the channel estimation process.

The additive mobility noise (MN) is defined as follows:

$$\boldsymbol{\Theta}^o_{mj}(z) = \sqrt{1-\varphi^2_{mj}} \sum_{f=1}^{z-1} \varphi^{z-f-1}_{mj} \mathbf{e}_{mj}(f) \qquad (9)$$

and $\mathbf{e}_{mj}(l)$ represents the randomly varying component. Note that each entry of $\mathbf{e}_{mj}(l)$ is i.i.d and follows $\mathcal{CN}(0, \sigma^2_{\mathbf{e}_{mj}})$. Additionally, the expectation for $\boldsymbol{\Theta}^o_{mj}(z)$ is zero, and its variance is expressed as

$$V\left\{\boldsymbol{\Theta}^o_{mj}(z)\right\} = \left(1-\varphi^2_{mj}\right)\sigma^2_{\mathbf{e}_{mj}}\varphi^{2(z-1)}_{mj} \sum_{l=1}^{z-1}\left(\varphi^{-2}_{mj}\right)^l,$$
$$= \sigma^2_{\mathbf{e}_{mj}}\left(1-\varphi^{2(z-1)}_{mj}\right). \qquad (10)$$

III. PERFORMANCE ANALYSIS
This section studies the performance of DL and UL links of the devised FD-CFm-MIMO system as given below.

A. DOWNLINK (DL) DATA TRANSMISSION
Initially, the unit-energy message symbol s^d_k and the power-control coefficient (η_{mk}) of the kth DL-VCU undergo scaling and subsequent quantization. Later, the CPU transmits the quantized symbol to the kth DL-VCU via the confined fronthaul link of the mth AP. Because of confined fronthaul

link capacity, the mth AP can serve only a subset of DL-VCUs, i.e., $\kappa_{dm} \subset \{1, \ldots, K_d\}$. By obtaining symbols from the CPU, AP transmits the signal after performing maximum-ratio transmission (MRT) precoding using MMSE channel estimation [16], [29], and thus, the resultant signal is given by

$$\mathbf{x}^d_m = \sqrt{\mu_d}\sum_{k\in\kappa_{dm}}\left(\hat{\mathbf{g}}^d_{mk}\right)^*\mathcal{Q}\left(\sqrt{\eta_{mk}}s^d_k\right),$$
$$= \sqrt{\mu_d}\sum_{k\in\kappa_{dm}}\left(\hat{\mathbf{g}}^d_{mk}\right)^*\left(\tilde{a}\sqrt{\eta_{mk}}s^d_k + \varsigma^d_{mk}\right). \qquad (11)$$

where μ_d and $\eta_{mk}, \forall m \in \mathcal{M}, k \in \mathcal{K}_d$ represent the maximum normalized AP transmit power and the power control coefficient, respectively. Here, $(\hat{\mathbf{g}}^d_{mk})^*$ indicates the conjugate of the $(\hat{\mathbf{g}}^d_{mk})$ and $\mathcal{Q}(\cdot)$ denotes the quantization operator, which is a function of an additive distortion ς^d_{mk} and scalable attenuation $\tilde{a}$. Let $\mathbb{E}\{(\varsigma^d_{mk})^2\} = (\tilde{b}-\tilde{a}^2)\eta_{mk}$ be the variance of ς^d_{mk} with constants $\tilde{a}$ and $\tilde{b}$, which depends on the quantity of fronthaul quantization bits [17]. Based on the constraint of mean-normalized power, i.e., $\mathbb{E}\{|\mathbf{x}^d_m|^2\} \leq \mu_d$, the single-AP power constraint is defined as

$$\tilde{b}\sum_{k\in\mathcal{K}_d}\sigma^2_{d,mk}\eta_{mk} \leq \frac{1}{N_{tx}}, \forall m, \qquad (12)$$

where $\tilde{b}$ is a constant that depends on the quantity of fronthaul quantization bits. The set $\mathcal{M}^d_k$ is a subset of all APs represented by integers from 1 to M. Each AP in $\mathcal{M}^d_k$ transmits the required message signal to the kth DL-VCU as well as several distortion and interference factors. The kth DL-VCU is served by the mth AP if k belongs to the set κ_{dm}, which is true if and only if m belongs to $\mathcal{M}^d_k$. The kth DL-VCU received signal is expressed as

$$y^d_k = \sum_{m=1}^{M}\left(\mathbf{g}^d_{mk}\right)^T\mathbf{x}^d_m + \sum_{l=1}^{K_u}h_{kl}x^u_l + w^d_k$$
$$= \underbrace{\tilde{a}\sqrt{\mu_d}\sum_{m\in\mathcal{M}^d_k}\sqrt{\eta_{mk}}\left(\mathbf{g}^d_{mk}\right)^T\left(\hat{\mathbf{g}}^d_{mk}\right)^*s^d_k}_{\text{desired signal, DS}^d_k}$$
$$+ \underbrace{\tilde{a}\sqrt{\mu_d}\sum_{m=1}^{M}\sum_{q\in\kappa_{dm}\backslash k}\sqrt{\eta_{mq}}\left(\mathbf{g}^d_{mk}\right)^T\left(\hat{\mathbf{g}}^d_{mq}\right)^*s^d_q}_{\text{inter-user interference, IUI}^d_k}$$

$$+ \sqrt{\mu_d} \underbrace{\sum_{m=1}^{M} \sum_{q \in \kappa_{dm}} \left(\mathbf{g}_{mk}^d\right)^T \left(\hat{\mathbf{g}}_{mq}^d\right)^* \varsigma_{mq}^d}_{\text{total quantization distortion,TQD}_k^d}$$

$$+ \underbrace{\sum_{l=1}^{K_u} h_{kl} x_l^u}_{\text{co-channel interference ,CCI}_k^d} + \underbrace{w_k^d}_{\text{AWGN at receiver,W}_k^d} . \quad (13)$$

B. UPLINK (UL) DATA TRANSMISSION

Due to the FD nature of all APs, the K_u UL-VCUs simultaneously transmit signals to all M APs utilizing the same spectrum resource used for DL transmission. The lth UL-VCU transmits a signal $x_l^u = \sqrt{\mu_u \Omega_l} s_l^u$, where s_l^u, Ω_l and μ_u are the unit-energy message symbol, the power coefficient of UL transmission and the UL transmit signal-to-noise ratio (SNR) of maximum value, respectively. In order to meet the normalized SNR requirement, $\mathbb{E}\{|x_l^u|^2\} \leq \mu_u$, the lth UL-VCU must adhere to the following constraint, $0 \leq \Omega_l \leq 1$. The UL signal received at the mth AP is presented as

$$\mathbf{y}_m^u = \left[\sum_{l=1}^{K_u} \mathbf{g}_{ml}^u x_l^u + \sum_{i=1}^{M} \mathbf{H}_{mi} \mathbf{x_i}^d + \mathbf{w}_m^u \right], \quad (14)$$

where $\mathbf{w}_m^u \in \mathbb{C}^{N_r \times 1} \sim \mathcal{CN}(0, \sigma_n^2)$ represents the i.i.d. entries of additive white Gaussian noise at the mth AP. In our approach, we aim to estimate and partially minimize inter and intra-AP interference with a minimal increase in pilot overhead. While it is acknowledged that complete cancellation of such interference would impose significant pilot overhead, front-haul signaling, and computational complexity, our method focuses on achieving a practical balance that is more suitable for URLLC systems. Note that $\mathbf{H}_{mi} \in \mathbb{C}^{N_r \times N_t}$ denotes the residual interference (RI) channel for inter-/intra-AP [15]. Here, each entry of $\mathbf{H}_{mi}$ is i.i.d and follows $\mathcal{CN}(0, \gamma_{\text{RI},mi})$, where γ_{RI} denotes the suppressed RI power.

After receiving signals from every UL-VCU, the mth AP executes maximum-ratio combining (MRC) for the lth UL-VCU with $(\hat{\mathbf{g}}_{ml}^u)^H$. As the fronthaul is confined, firstly, the AP performs quantization on the resultant signal and then sends it to CPU; secondly, a subset of APs, i.e., $\mathcal{M}_l^u \subset \{1, \ldots, M\}$ serving the lth UL-VCU send contributions to the CPU. The mth AP serves a particular subset of UL-VCUs,[2] which is denoted as $\kappa_{um} \subset \{1, \ldots, K_u\}$. A lth UL-VCU is served by the mth AP if and only if l belongs to κ_{um}, which is equivalent to m being a member of the set of APs $\mathcal{M}_l^u$. The

CPU obtains the signal corresponding to the lth UL-VCU as follows

$$y_l^u = \sum_{m \in \mathcal{M}_l^u} \mathcal{Q}\left(\left(\hat{\mathbf{g}}_{ml}^u\right)^H \mathbf{y}_m^u\right)$$

$$= \tilde{a} \underbrace{\sum_{m \in \mathcal{M}_l^u} \sqrt{\mu_u \Omega_l} (\hat{\mathbf{g}}_{ml}^u)^H \mathbf{g}_{ml}^u s_l^u}_{\text{desired signal, DS}_l^u}$$

$$+ \tilde{a} \underbrace{\sum_{m \in \mathcal{M}_l^u} \sum_{q=1, q \neq l}^{K_u} \sqrt{\mu_u \mu_q} (\hat{\mathbf{g}}_{ml}^u)^H \mathbf{g}_{mq}^u s_q^u}_{\text{inter-user interference, IUI}_l^u}$$

$$+ \tilde{a} \underbrace{\sum_{m \in \mathcal{M}_l^u} \sum_{i=1}^{M} \sqrt{\mu_d} \sum_{k \in \kappa_{di}} (\hat{\mathbf{g}}_{ml}^u)^H \mathbf{H}_{mi} \left(\hat{\mathbf{g}}_{ik}^d\right)^* \left(\tilde{a}\sqrt{\eta_{ik}} s_k^d + \varsigma_{ik}^d\right)}_{\text{residual interference (inter-AP and intra-AP), RI}_l^u}$$

$$+ \tilde{a} \underbrace{\sum_{m \in \mathcal{M}_l^u} (\hat{\mathbf{g}}_{ml}^u)^H \mathbf{w}_m^u}_{\text{AWGN at APs, W}_l^u} + \underbrace{\sum_{m \in \mathcal{M}_l^u} \varsigma_{ml}^u}_{\text{total quantization distortion, TQD}_l^u} . \quad (15)$$

After considering time-selective fading[3] and substituting the (8) in (13) and (15), we get the signal-to-interference-plus-noise ratio (SINR) of the kth DL-VCU and the lth UL-VCU respectively, is presented as

$$\Gamma_j^o = N_j^o \Big/ I_j^o, \quad (16)$$

where $N_j^o = |\sum_{m \in \mathcal{M}_j^o} \frac{C_{mj}}{\sqrt{N_t}} \varphi_{mj}^{2(z-1)} (\hat{\mathbf{g}}_{mj}^d(1))^H \hat{\mathbf{g}}_{mj}^d(1)|^2$, $j \in \{k, l\}$, $o \in \{d, u\}$, I_j^o is the interference plus noise term. Here,

$$C_{mk} = \tilde{a} \sqrt{\frac{P_d}{k_{dm}M}} \sqrt{\eta_{mk}} \beta_{mk}, \quad (17)$$

$$C_{ml} = \tilde{a} \sqrt{\frac{P_u}{k_{ul}M}} \sqrt{\Omega_l} \beta_{ml}, \quad (18)$$

$$I_k^d = \left|\text{IUI}_k^d\right|^2 + \left|\text{UDI}_k^d\right|^2 + \left|\text{W}_k^d\right|^2 + \left|\text{TQD}_k^d\right|^2 + \left|\text{MN}_k^d\right|^2, \quad (19)$$

$$I_l^u = \left|\text{IUI}_l^u\right|^2 + \left|\text{RI}_l^u\right|^2 + \left|\text{W}_l^u\right|^2 + \left|\text{TQD}_l^u\right|^2. \quad (20)$$

C. CUMULATIVE DISTRIBUTION FUNCTION (CDF) OF Γ_J^O

In order to obtain the CDF of Γ_j^o, $\forall j \in \{k, l\}$, $o \in \{d, u\}$, we first use the approximate the distribution of the products of random vectors, i.e., $|\frac{1}{\sqrt{N_t}} \hat{\mathbf{g}}_{mk}^d(1)^H \hat{\mathbf{g}}_{mk}^d(1)|^2$ and $|\frac{1}{\sqrt{N_t}} \hat{\mathbf{g}}_{mk}^d(1)^H \hat{\mathbf{g}}_{mq}^d(1)|^2$, in (16) as follows [30], [31]

$$\left|\frac{1}{\sqrt{N_t}} \hat{\mathbf{g}}_{mk}^d(1)^H \hat{\mathbf{g}}_{mk}^d(1)\right|^2 \sim \mathcal{G}(N_t, 1/N_t), \quad (21)$$

$$\left|\frac{1}{\sqrt{N_t}} \hat{\mathbf{g}}_{mk}^d(1)^H \hat{\mathbf{g}}_{mq}^d(1)\right|^2 \sim \mathcal{G}(1, 1), \quad \forall k \neq q, \quad (22)$$

where $\mathcal{G}(.)$ denotes gamma distribution. Therefore, similar to [31], the distribution of numerator (N_j^o) and denominator

---

[2]The algorithm for the selection of APs, UL-VCUs and DL-VCUs is given in [16]. In our FD CF-mMIMO system, APs receive signals from all UL-UEs but selectively transmit contributions from a subset to the CPU, based on a proportionately fair selection criteria [16]. This ensures efficient fronthaul utilization and optimal service quality, even under the constraints of user mobility and imperfect CSI.

[3]Note that time-selective fading introduces mobility noise (MN).

(I_j^o) of (16) can be represented in terms of Gamma random variables and further assessed using the Welch-Satterthwaite approximation[4] [19] as shown below

$$N_j^o \sim \sum_{m \in \mathcal{M}_j^o} \mathcal{G}\left(N_t, \left(\frac{C_{mj}}{\sqrt{N_t}}\varphi_{mj}^{2(z-1)}\right)^2\right), \quad (23)$$

where $C_{mkq} = \tilde{a}\sqrt{\frac{P_d}{k_{dm}M}}\sqrt{\eta_{mk}}\beta_{mk}^{1/2}\beta_{mq}^{1/2}$, $D_{mkq} = \sqrt{\frac{P_d}{k_{dm}M}}\varsigma_{mq}^d$, $E_u = \sqrt{\mu_u \Omega_l}$, $\mu_u = \frac{P_u}{k_{ul}MN_t}$, $C_{ml} = \tilde{a}\sqrt{\frac{P_u}{k_{ul}M}}\sqrt{\Omega_l}\beta_{ml}$, $D_{ml} = \tilde{a}\sqrt{\frac{P_u}{k_{ul}M}}\beta_{ml}^{1/2}\beta_{mq}^{1/2}\sqrt{\mu_q}$, $E_m = \tilde{a}\sqrt{\frac{P_d}{k_{dm}M}}\sqrt{\eta_{ik}}$, $G_m = \tilde{a}\beta_{ml}^{1/2}$, $F_m = \tilde{a}\sqrt{\frac{P_d}{k_{dm}M}}$.

Here, the crucial parameters $\tilde{a}$ and $\varsigma_{mq}^o, \forall o \in \{d, u\}$ play a pivotal role in determining fronthaul capacity, while $\varphi_{mq}^o, \forall o \in \{d, u\}$ characterizes the VCU's velocity and DPS model, influencing channel conditions. These insights are extensively explored in the numerical results section, shedding light on their impact on system performance.

Now, we further simplify the Γ_j^o in (16) as follows

$$\Gamma_k^d = \frac{X}{Y + \sigma_k^2}, \quad \Gamma_l^u = \frac{X}{Y}. \quad (26)$$

where $X = N_j^d$ and $Y = I_k^d - \sigma_k^2$ when $o = d$, and $X = N_j^u$ and $Y = I_l^u$ when $o = u$. Thus, from (23), we get

$$X \sim \sum_{m \in \mathcal{M}_k^d} \mathcal{G}(\Lambda_1, \varrho_1), \quad \Lambda_1 = N_t, \quad \varrho_1 = \left(\frac{C_{mj}}{\sqrt{N_t}}\varphi_{mj}^{2(z-1)}\right)^2.$$

When M and K values are significantly high, the value of Y greatly exceeds σ^2, leading to the expression $\Gamma_k^d = X/Y$ in the DL case. Additionally, it is possible to express Y as the sum of all the denominator terms using the gamma distribution, which is similar to the representation of the numerator term X.

Using [12, Lemmas 2 and 3], X and Y of DL expression in (26) can be further simplified as follows:

$$X \sim \mathcal{G}(\Lambda_x, \varrho_x) = \mathcal{G}_1, Y \sim \mathcal{G}(\Lambda_y, \varrho_y) = \sum_{i=2}^{6} \mathcal{G}_i, \quad (27)$$

---

[4]The Welch-Satterthwaite approximation is employed due to its adeptness at handling complex data distributions and its adaptability for various sample sizes, providing a more accurate estimation of outage probability for our URLLC-enabled FD CF-mMIMO system model.

where

$$\Lambda_x = \frac{E\{X\}^2}{V\{X\}}, \quad (28)$$

$$\Lambda_y = \frac{E\{Y\}^2}{V\{Y\}}, \quad (29)$$

$$\varrho_x = \frac{V\{X\}}{E\{X\}}, \quad (30)$$

$$\varrho_y = \frac{V\{Y\}}{E\{Y\}}. \quad (31)$$

The expectation and variance of X are calculated as follows:

$$E\{X\} = \sum_{m \in \mathcal{M}_k^d} \Lambda_1 \varrho_1, \quad (32)$$

$$V\{X\} = \sum_{m \in \mathcal{M}_k^d} \Lambda_1 \varrho_1^2. \quad (33)$$

Similarly, the expectation and variance of Y are calculated in the (34) and (35), respectively, shown at the bottom of the next page. Note that $E\{.\}$ and $V\{.\}$ represent the expectation and variance of Gamma random variables, and the UL expression in (26) can be simplified as similar to the DL simplification. By considering $\Gamma_j^o \in \{\Gamma_k^d, \Gamma_l^u\}$, $X \in \mathcal{G}(\Lambda_x, \varrho_x)$ and $Y \in \mathcal{G}(\Lambda_y, \varrho_y)$, the CDF of the Γ_j^o is expressed as

$$F_{\Gamma_j^o}(\mathfrak{b}) = P\left(\Gamma_j^o \le \mathfrak{b}\right) = P\left(\frac{X}{Y} \le \mathfrak{b}\right)$$
$$= \int_0^\infty \frac{\gamma\left(\Lambda_x, \frac{\mathfrak{b}y}{\varrho_x}\right)}{\Gamma(\Lambda_x)}\frac{x^{\Lambda_y-1}e^{-x/\varrho_y}}{\Gamma(\Lambda_y)\varrho_y^{\Lambda_y}}dy, \quad (36)$$

where $\Gamma(.)$ is the gamma function and $\gamma(.)$ is the upper incomplete gamma function [32, eq. (6.5.3)]. Here, $\mathfrak{b}$ denotes the SINR threshold. Let $I' = \int_0^\infty \gamma\left(\Lambda_x, \frac{\mathfrak{b}y}{\varrho_x}\right)x^{\Lambda_y-1}e^{-x/\varrho_y}dy$. By using the relation given in [33, eq. (6.455.1)], the integral term I' in (36) can be solved. Therefore, by using the hypergeometric function $_2F_1$, the closed-form expression for the CDF $F_{\Gamma_j^o}(\mathfrak{b})$ is given by

$$F_{\Gamma_j^o}(\mathfrak{b}) = \frac{\mathfrak{b}^{\Lambda_x}\Gamma\left(\Lambda_y + \Lambda_x\right)}{\Gamma(\Lambda_x)\varrho_x^{\Lambda_x}\Gamma(\Lambda_y)\varrho_y^{\Lambda_y}\Lambda_x\left(\frac{\mathfrak{b}}{\varrho_x} + \frac{1}{\varrho_y}\right)^{\Lambda_y + \Lambda_x}}$$

$$I_k^d \sim \left(\begin{array}{c}\sum_{m \in \mathcal{M}_k^d}\sum_{k \in k_{dm}}\mathcal{G}\left(N_t, \left(\frac{C_{mk}}{\sqrt{N_t}}\right)^2\sigma_{emk}^2\left(1 - \varphi_{mk}^{2(z-1)}\right)\right) + \sum_{m \in \mathcal{M}}\sum_{q \in k_{dm}\setminus k}\mathcal{G}\left(1, \left(C_{mk}\varphi_{mk}^{(z-1)}\varphi_{mq}^{(z-1)}\right)^2\right) \\ + \sum_{l \in k_u}\mathcal{G}\left(1, \mu_u\Omega_l\beta_{kl}^2\right) + \sum_{m \in \mathcal{M}}\sum_{q \in \kappa_{dm}}\mathcal{G}\left(1, \left(\varphi_{mk}^{(z-1)}\varphi_{mq}^{(z-1)}D_{mkq}\right)^2\right) + \sum_{m \in \mathcal{M}}\sum_{q \in \kappa_{dm}}\mathcal{G}\left(1, D_{mkq}^2\right) + \sigma_k^2\end{array}\right), \quad (24)$$

$$I_l^u \sim \left(\begin{array}{c}\sum_{m \in \mathcal{M}_l^u}\sum_{q \in k_u}\mathcal{G}\left(N_t, \left(\frac{C_{ml}}{\sqrt{N_t}}\right)^2\sigma_{emk}^2\left(1 - \varphi_{mk}^{2(z-1)}\right)\right) + \sum_{m \in \mathcal{M}_l^u}\sum_{q \in k_u\setminus l}\mathcal{G}\left(1, \left(D_{ml}\varphi_{ml}^{(z-1)}\varphi_{mq}^{(z-1)}\right)^2\right) \\ + \sum_{m \in \mathcal{M}_l^u}\sum_{i=1}^{M}\sum_{k \in \kappa_d}\mathcal{G}\left(1, E_m^2\beta_{ml}\beta_{ik}\right) + \sum_{m \in \mathcal{M}_l^u}\sum_{i=1}^{M}\sum_{k \in \kappa_d}\mathcal{G}\left(1, F_m^2\beta_{ml}\beta_{ik}\left(\tilde{b} - \tilde{a}\right)^2\eta_{mk}\right) \\ + \sum_{m \in \mathcal{M}_l^u}\mathcal{G}\left(1, G_m^2\sigma_{emnk}^2\varphi_{ml}^{2(z-1)}\right) + \sum_{m \in \mathcal{M}_l^u}\mathcal{G}\left(1, \left(\tilde{b} - \tilde{a}\right)^2\eta_{mk}\right)\end{array}\right). \quad (25)$$

$$\times {}_2F_1\left(1, \Lambda_y + \Lambda_x; \Lambda_y + 1; \frac{1/\varrho_y}{\frac{b}{\varrho_x} + \frac{1}{\varrho_y}}\right). \quad (37)$$

D. OUTAGE PROBABILITY (OP)

For the case of infinite block-length, the OP for the jth VCU is defined as the probability such that Γ_j^o falls below a predefined threshold γ_{th} and is given by

$$P_{\text{out.m}}^{(j)} = P\left(\Gamma_j^o < \gamma_{\text{th}}\right) = F_{\Gamma_j^o}(\gamma_{\text{th}}). \quad (38)$$

Substituting (37) in (38), the final closed-form expression of the OP is obtained as

$$P_{\text{out.m}}^{(j)} = \frac{\gamma_{th}{}^{\Lambda_x}\Gamma\left(\Lambda_y + \Lambda_x\right)}{\Gamma(\Lambda_x)\varrho_x{}^{\Lambda_x}\Gamma\left(\Lambda_y\right)\varrho_y{}^{\Lambda_y}\Lambda_y\left(\frac{\gamma_{th}}{\varrho_x} + \frac{1}{\varrho_y}\right)^{\Lambda_y + \Lambda_x}}$$
$$\times {}_2F_1\left(1, \Lambda_y + \Lambda_x; \Lambda_y + 1; \frac{1/\varrho_y}{\frac{\gamma_{th}}{\varrho_x} + \frac{1}{\varrho_y}}\right). \quad (39)$$

The derived outage probability expression highlights a distinct relationship among system parameters, specifically the signal-to-noise ratio, VCU density, and AP density. Notably, under infinite power regime (asymptotic analysis[5]), i.e., $P_d \to \infty$ and $P_u \to \infty$, it becomes evident from the simulation results in Fig. 8 and Fig. 9 that the OP is notably and inversely impacted by the density of APs.

E. BLOCK ERROR RATE (BLER)

For a finite block-length analysis, we consider each packet transmission with b number of information bits over the g number of channel uses. The coding rate $r_j = b/g_j$ where $j \in \{k, l\}$, where g_j specifically denotes the number of channel uses for the jth link. Let ϵ_k and ϵ_l represent the BLER of DL and UL links, respectively. When compared to a deterministic channel with the same capacity, the channel's stochastic variability is measured by the channel dispersion given by $V(\Gamma_j^o) = (1 - (1 + \Gamma_j^o))^{-2}(\log_2(e))^2$. It is observed that ϵ_j can be tightly approximated as in [10] as $\epsilon_j(r_j) \approx E\left\{Q(\frac{C(\Gamma_j^o) - r_j}{\sqrt{V(\Gamma_j^o)/g_j}})\right\}$ where $C(\Gamma_j^o) = \log_2(1 + \Gamma_j^o)$ is the

---

[5]We adopt the asymptotic analysis which resembles that presented in [12].

Shannon capacity. It is mathematically intractable to evaluate ϵ (i.e., $\epsilon_j(r_j)$) in closed form, and hence we use the linear approximation of $Q(\frac{C(\Gamma_j^o) - r_j}{\sqrt{V(\Gamma_j^o)/g_j}}) \approx K(\Gamma_j^o)$ [10], as

$$K\left(\Gamma_j^o\right) = \begin{cases} 1, & \text{if } \Gamma_j^o \leq \varsigma_j, \\ \frac{1}{2} - \phi_j\sqrt{g_j}\left(\Gamma_j^o - \phi_j\right), & \text{if } \varsigma_j < \Gamma_j^o < \xi_j, \quad (40) \\ 0, & \text{if } \Gamma_j^o \geq \xi_j, \end{cases}$$

where $\phi_j = \frac{1}{2\pi\sqrt{2^{2r_j}-1}}$, $\phi_j = 2^{r_j} - 1$, $\varsigma_j = \phi_j - \frac{1}{2\phi_j\sqrt{g_j}}$, $\xi_j = \phi_j + \frac{1}{2\phi_j\sqrt{g_j}}$.

We evaluate the BLER of link j as $\epsilon_j(r_j) \approx \int_0^\infty K(x)f_{\Gamma_j^o} dx$. Thus,

$$\epsilon_j(r_j) \approx \left[K(x)F_{\Gamma_j^o}\right]_0^\infty - \int_0^\infty F_{\Gamma_j^o}(x)dK(x), \quad (41)$$

where $F\{\cdot\}$ is the CDF. We further simplify ϵ_j through the differentiation of $K(x)$ and substituting it in (41) as presented below $\epsilon_j(r_j) \approx \phi_j\sqrt{g_j}\int_{\varsigma_j}^{\xi_j} F_{\Gamma_j^o}(x) dx$. Finally, Gaussian-Chebyshev quadrature method [10] is applied on ϵ_j to obtain the following

$$\epsilon_j(r_j) = \left(\frac{\xi_j - \varsigma_j}{2}\right)\sum_{z=1}^Z \frac{\pi}{Z}\sqrt{1 - \varnothing_z^2}F_{\Gamma_j^o}(w) + R_Z, \quad (42)$$

where Z denotes accuracy-complexity trade-off parameter, $\varnothing_z = \cos(\frac{(2z-1)\pi}{2Z})$, $w = ((\xi_z + \varsigma_z)/2 + \varnothing_z(\xi_z - \varsigma_z)/2)$, R_Z are the error terms ($R_Z = 0$ for higher Z value). Finally, the OP for the j and m links is defined as $P_{out.m} = \epsilon_{j.m}(\gamma_{th})$ [10]. Thus, the OP for the devised system with URLLC can be expressed as

$$P_{\text{out.total}}^{(j)} = \prod_{m=1}^M \epsilon_{j.m}(\gamma_{th}). \quad (43)$$

The expression for the outage probability in (43) provides key insights into the role of channel dispersion, coding rate, and the accuracy-complexity trade-off in URLLC system reliability. It's worth noting that as depicted in Fig. 3, Fig. 4, and Fig. 5, the outage probability demonstrates a notable decline with an increase in the parameter M, highlighting the positive impact of higher M values on system reliability.

$$E\{Y\} = \sum_{i=2}^6 E\{\mathcal{G}_i\} = \sum_{m \in \mathcal{M}_k^d}\sum_{k \in k_{dm}} \Lambda_2\varrho_2 + \sum_{m \in \mathcal{M}}\sum_{q \in k_{dm}} \Lambda_3\varrho_3 + \sum_{l \in k_u} \Lambda_4\varrho_4$$
$$+ \sum_{m \in \mathcal{M}}\sum_{q \in k_{dm}} \Lambda_5\varrho_5 + \sum_{m \in \mathcal{M}}\sum_{q \in k_{dm}} \Lambda_6\varrho_6, \quad (34)$$

$$V\{Y\} = \sum_{i=2}^6 V\{\mathcal{G}_i\} = \sum_{m \in \mathcal{M}_k^d}\sum_{k \in k_{dm}} \Lambda_2\varrho_2^2 + \sum_{m \in \mathcal{M}}\sum_{q \in k_{dm}} \Lambda_3\varrho_3^2 + \sum_{l \in k_u} \Lambda_4\varrho_4^2$$
$$+ \sum_{m \in \mathcal{M}}\sum_{q \in k_{dm}} \Lambda_5\varrho_5^2 + \sum_{m \in \mathcal{M}}\sum_{q \in k_{dm}} \Lambda_6\varrho_6^2. \quad (35)$$

F. ASYMPTOTIC ANALYSIS ($M \to \infty$, $N \to \infty$)

We first consider the UL transmission (15). Using (8), we can write

$$\sum_{m=1}^{M} \sqrt{\Theta_q}(\hat{\mathbf{g}}_{m\ell}^{u})^{H}\mathbf{g}_{mq}^{u}$$

$$= \tilde{a} \sum_{m \in \mathcal{M}_{l}^{u}} \sqrt{\Theta_{l}\beta_{ml}\beta_{mq}}\rho_{ml}^{2(z-1)}(\hat{\mathbf{g}}_{ml}^{u}(1))^{H}\hat{\mathbf{g}}_{mq}^{u}(1)$$

$$+ \tilde{a} \sum_{m \in \mathcal{M}_{l}^{u}} \sqrt{\Theta_{l}}(\boldsymbol{\phi}_{ml}(1))^{H}\hat{\boldsymbol{\phi}}_{mq}(1). \quad (44)$$

From (44) and Tchebyshev's theorem [34]

$$\frac{1}{M}\text{DS}_{\ell}^{u} - \frac{1}{M}\left(\frac{\tilde{a}\sqrt{N_{t}P_{u}\Theta_{l}}}{\sqrt{k_{ul}}}\rho_{ml}^{2(z-1)}\right) \xrightarrow[M,N\to\infty]{P} 0, \quad (45)$$

$$\frac{1}{M}\text{IUI}_{\ell}^{u} \xrightarrow[M,N\to\infty]{P} 0, \quad (46)$$

$$\frac{1}{M}\text{W}_{\ell}^{u} \xrightarrow[M,N\to\infty]{P} 0, \quad (47)$$

$$\frac{1}{M}\text{TQD}_{l}^{u} \xrightarrow[M,N\to\infty]{P} 0, \quad (48)$$

where DS_{ℓ}^{u}, IUI_{ℓ}^{u}, N_{ℓ}^{u}, and TQD_{l}^{u} are given in (15), and $\xrightarrow[M,N\to\infty]{P}$ denotes the convergence in probability when $M, N \to \infty$. Similarly, we have RI_{ℓ}^{u} from (15) as $\text{RI}_{\ell}^{u} = \tilde{a}\sum_{m \in \mathcal{M}_{l}^{u}}\sum_{i=1}^{M}\sqrt{P_{d}}\sum_{k \in \kappa_{di}}(\hat{\mathbf{g}}_{ml}^{u})^{H}\mathbf{H}_{mi}(\hat{\mathbf{g}}_{ik}^{d})^{*}(\tilde{a}\sqrt{\eta_{ik}}s_{k}^{d}+\varsigma_{ik}^{d})$. Let us consider $RI' = \tilde{a}(\hat{\mathbf{g}}_{ml}^{u})^{H}\mathbf{H}_{mi}(\hat{\mathbf{g}}_{ik}^{d})^{*}(\tilde{a}\sqrt{\eta_{ik}}s_{k}^{d}+\varsigma_{ik}^{d})$, which is a zero-expectation random variable and its variance is calculated as $V(RI') = \sigma_{\text{RI},mik}^{2}(\tilde{a}\eta_{ik}+(\tilde{b}-\tilde{a}^{2}))$. Using RI_{ℓ}^{u} and $V(RI')$, and applying Lyapunov central limit theorem [34], we get

$$\frac{1}{M}\text{RI}_{\ell}^{u} \xrightarrow[M,N\to\infty]{d} \frac{1}{M}\sqrt{P_{d}}$$

$$\sum_{k \in \mathcal{K}_{d}}\sqrt{\sum_{m=1}^{M}\sum_{i \in \mathcal{M}}\sigma_{\text{RI},mik}^{2}\left(\tilde{a}\eta_{ik}+\left(\tilde{b}-\tilde{a}^{2}\right)\right)}z_{k}s_{k}^{d}, \quad (49)$$

where small $\xrightarrow[M,N\to\infty]{d}$ denotes convergence in distribution when $M, N \to \infty$ and z_{k} is a $\mathcal{CN}(0,1)$ RV. Similar results hold for the DL transmission as small $\frac{1}{M}\text{DS}_{k}^{d} - \frac{1}{M}(\frac{\tilde{a}\sqrt{N_{t}P_{d}\eta_{mk}}}{\sqrt{\kappa_{dm}}}\rho_{mk}^{2(z-1)}) \xrightarrow[M,N\to\infty]{P} 0$, $\frac{1}{M}\text{IUI}_{k}^{d} \xrightarrow[M,N\to\infty]{P} 0$, $\frac{1}{M}\text{TQD}_{k}^{d} \xrightarrow[M,N\to\infty]{P} 0$, $\frac{1}{M}\text{UDI}_{k}^{d} \xrightarrow[M,N\to\infty]{P} 0$. It can be seen from (46)-(49) that when $M, N \to \infty$, the channels between the APs and the UEs become orthogonal. Using conjugate beamforming and matched filtering, the RI persists while multi-UE interferences and noise disappear. Therefore, the RI is the main limitation of the CF-mMIMO systems. However, this limitation can be overcome by choosing an appropriate power control method. Now, we use Lindeberg-Lévy central limit theorem (CLT) [34], which is a stronger version of the CLT to analyze the convergence of the sum of i.i.d. random variables of RI_{ℓ}^{u}. Note that, all the i.i.d. random variables of RI_{ℓ}^{u} are with finite mean and variance and thus its sum

TABLE 3. Simulation parameters.

Parameter	value
Threshold SINR γ_{th}	5 dB
V_{mp} (mph) [10], [11]	0, 30
Number of antennas (N_t or N_r)	10
σ_{th}	8 dB
Path loss exponent	2
Number of VCUs (K)	40, 60
Symbol rate (R_s) [10]	9.6 kbps
D, d_0, d_1 [11]	1 Km, 0.01 Km, 0.05 Km
Frequency of the carrier (f) [10]	1.9 GHZ
Number of APs (M)	[100, 50]
Coherence time interval (T)	1 ms
Length of coherence period	200 symbols
$[\tau_u, \tau_d]$	[40, 40]
Length of transmission of block (g_j)	300

converges in distribution to a standard normal distribution as $M, N \to \infty$. Therefore, using Lindeberg-Lévy CLT and Tchebyshev's theorem along with η_{mk} in (49), we can write

$$\frac{1}{M}\text{RI}_{\ell}^{u} \xrightarrow[M,N\to\infty]{d} \frac{1}{M^{3/2}}\sqrt{P_{d}} \sum_{k \in \mathcal{K}_{d}}\hat{z}_{k}s_{k}^{d} \xrightarrow[M,N\to\infty]{} 0, \quad (50)$$

$$\frac{1}{\sqrt{M}}\text{DS}_{k}^{d} \xrightarrow[M,N\to\infty]{P} 0, \quad (51)$$

where $\hat{z}_{k} \sim \mathcal{CN}(0, \frac{\sum_{m=1}^{M}\sum_{i \in \mathcal{M}}\sigma_{\text{RI, mik}}^{2}}{\sum_{k \in \mathcal{K}_{d}}\sigma_{\hat{\mathbf{g}}_{mk}^{d}}^{2}})$. Here, (50) and (51) demonstrate that as $M, N \to \infty$, by scaling the power coefficients appropriately, the RI can be mitigated while the DL transmission is not significantly affected.

IV. SIMULATION RESULTS

This section presents the OP for the devised system for varying K, P_d, N, and M. We assume all the M APs and K VCUs are randomly distributed over a square of area $D \times D \ km^2$. Table 3 outlines the simulation parameters used in numerical results.

Fig. 2 demonstrates the impact of DL power (P_d) on OP for FD-UL and FD-DL by considering the Rectangular DPS model [11] and $K = 40$. Because of the increased DL SINR, the FD-DL OP is more effective at raising P_d. On the other hand, a considerable increase in residual self-interference (RSI) power causes FD-UL outage performance to diminish as P_d rises. Additionally, it has been noted that the performance during outages of FD-UL and FD-DL has significantly improved due to the diversity gain achieved by increasing M. For instance, when M doubles in FD-UL at $P_d = 0.1$ watts, OP reduces by 50.617%, enhancing URLLC UL reliability. In FD-DL, this results in an 84.114% OP decrease, strengthening the DL for URLLC's critical tasks.
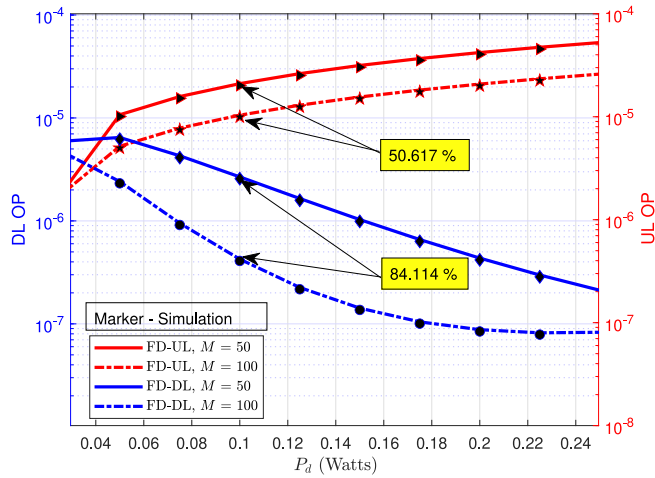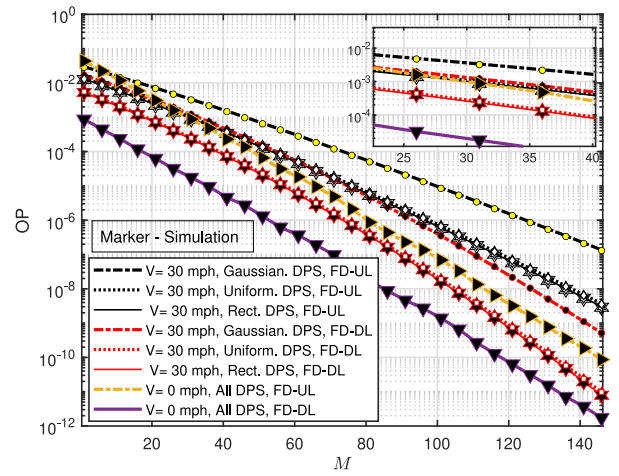
FIGURE 2. Effect of P_d on FD OP of the system for varying *M*.

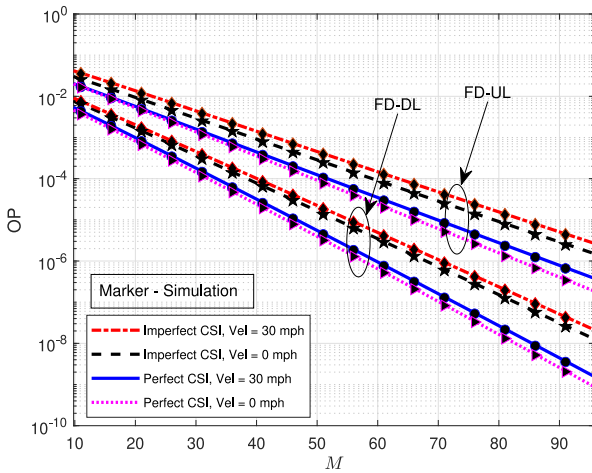**FIGURE 4.** Impact of different DPS models and time-selective fading.

FIGURE 3. Effect of CSI and mobility on the OP of the system.

Fig. 3 depicts the effect of the VCU mobility on the OP of the proposed system for different values of *M* considering both the imperfect CSI and perfect CSI scenarios. The CEE for the nth antenna of the mth AP to the kth VCU channel is defined as CEE = $E[||h_{mn} - \hat{h}_k||^2]$, where $\hat{h}_k$ indicates the estimated channel response corresponding to the exact channel response h_k, $k \in \{1, 2, 3, \ldots, K\}$. Compared to the perfect CSI, imperfect CSI with 20% CEE [10] degrades the OP significantly. Expectedly, the outage performance improves with an increase in the *M*, evincing the benefit of deploying a large number of distributed APs, which provides an adequate SINR to all VCUs. Further, the impact of VCU mobility can be observed in imperfect and perfect cases. As the time-selective fading does not impact the immobile VCUs, the outage performance is significantly better compared to the system involving consistent-speed VCUs. The system with immobile VCUs under the perfect CSI benefits from the minimal handover delay, whereas the system performance with mobile VCUs under an imperfect CSI scenario deteriorates as a result of handover delays.

In Fig. 4, we present an analysis of the impact of various DPS models namely, Gaussian DPS, Uniform DPS, and Rectangular DPS, on the OP for the proposed system. Considering VCUs in motion at consistent speed, i.e., 30 mph, the Rectangular DPS model exhibits superior performance compared to the Uniform and Gaussian DPS models concerning outage performance. For *M* =120 for FD-DL, we observe that the Rectangular DPS model has a 1×10^{-9} lower outage probability compared to the Uniform DPS model and 8.9×10^{-8} lower outage probability compared to the Gaussian DPS model. This disparity can be attributed to the diverse fading characteristics introduced by the Rectangular DPS model, which enables improved channel conditions for certain instances, enhancing the system's reliability. For *M* = 120, we observe that the Uniform DPS model has a 8.8×10^{-8} lower outage probability compared to the Gaussian DPS model because Uniform DPS introduces a wider range of Doppler shifts, accommodating a broader spectrum of potential signal variations due to VCU motion. This diversity can sometimes mitigate fading and interference, resulting in a more favorable OP compared to Gaussian DPS. Furthermore, an interesting trend emerges as the number of UL and DL VCUs increases. The system's OP degrades due to diminishing SINR, driven by the intensified interference from more active VCUs contending for limited resources. A similar OP trend is observed in FD-UL transmission. When the VCUs are stationary, corresponding to a velocity of 0 mph, the Doppler shift effect is eliminated. Consequently, the Rectangular, Uniform, and Gaussian DPS models all converge to a similar performance regarding OP. This is because, at 0 mph, the DPS models do not introduce any frequency dispersion caused by mobility, and thus, the fading characteristics are solely determined by the static channel conditions. As such, the previously observed disparities in OP among different DPS models mph for FD-DL and FD-UL transmissions are no longer present. The OP becomes independent of the DPS model used, as the channel conditions are not affected by the VCU mobility. Therefore,
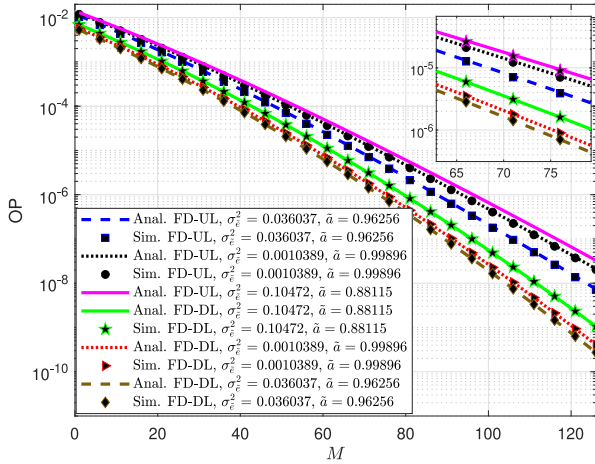
FIGURE 5. Effect of fronthaul quantization parameters on the OP of the system.
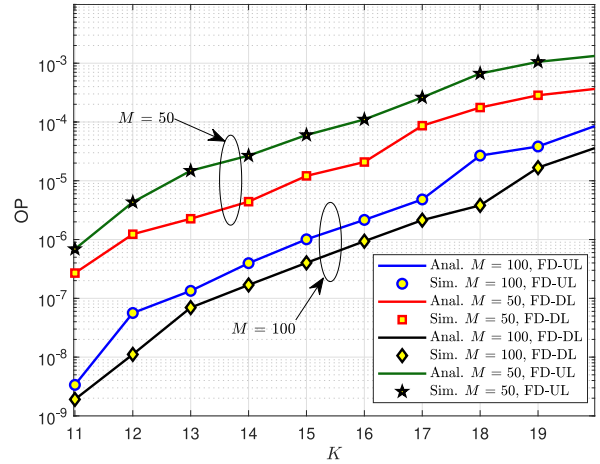

FIGURE 6. OP of FD-UL and FD-DL for varying number of VCUs (K).

the analysis in static conditions simplifies the evaluation of the system's performance, as the choice of the DPS model does not influence the OP.

The performance impact of confined fronthaul quantization parameters is illustrated in Fig. 5. The optimized values of the $\tilde{a}$ and $\tilde{\sigma}_e^2$ for the devised system are obtained from the [16, Table 2]. There are a few interesting observations revealed by the results of Fig. 5, which are discussed as follows. Based on the $\{\tilde{a}, \tilde{\sigma}_e^2\}$ values, there exist three optimized sets that constitute three different cases. Case 1: Worse outage performance is seen for higher $\tilde{\sigma}_e^2$ and lower $\tilde{a}$, i.e., $\{\tilde{a}_{low} = 0.8815, \tilde{\sigma}_{e_{high}}^2 = 0.10472\}$. Case 2: A moderate system performance is noticed for high $\tilde{a}$ and low $\tilde{\sigma}_e^2$, i.e., $\{\tilde{a}_{high} = 0.998, \tilde{\sigma}_{e_{low}}^2 = 0.0010389\}$. Case 3: The best outage performance is found for the moderate value of $\tilde{a}$ and moderate $\tilde{\sigma}_e^2$, i.e., $\{\tilde{a}_{mod} = 0.96256, \tilde{\sigma}_{e_{mod}}^2 = 0.036037\}$. Overall, we deduce that the moderate case of the optimal set of parameters taken into consideration (i.e., Case 3) offers improved outage performance under an immobile VCU scenario. These insights highlight the significance of carefully selecting these parameters to enhance system performance.

Fig. 6 compares the UL and DL outage performances of the devised system against K. The observed trend in the outage performances across increasing values of K can be attributed to the intricate interplay between signal quality, interference, and resource availability. As K rises, the network experiences a higher concentration of active VCUs, resulting in intensified interference due to simultaneous transmissions. This increased interference adversely affects the SINR, subsequently causing a reduction in the achievable data rates. As SINR diminishes, the likelihood of successful communication decreases, leading to an elevated OP. This trend underscores the challenge of maintaining reliable links in congested scenarios. Conversely, when the number of APs serving fewer VCUs increases, resource allocation becomes more efficient, and interference is mitigated, leading to improved SINR, data rates, and consequently reduced OP. This phenomenon emphasizes the importance of judiciously
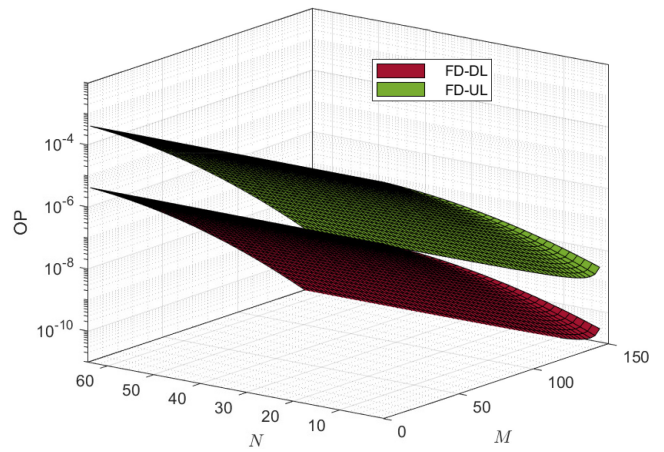

FIGURE 7. Impact of N and M on the OP of the proposed system.

managing network density and resource allocation to ensure reliable vehicular communication, especially under challenging conditions.

Figure 7 portrays a pivotal analysis of the impact of the number of APs and the number of antennas at each AP on the system's outage performance. Two significant observations emerge. Firstly, an increase in the number of antennas, denoted as N, results in elevated signal power. This phenomenon contributes to a notable reduction in the outage probabilities for both UL and DL transmissions. This is primarily attributed to the augmented signal strength, which improves the overall communication reliability. Secondly, the interplay between the number of antennas and system performance becomes more nuanced. With an increase in the number of antennas, represented by M, the system experiences enhanced diversity gain. This gain is a consequence of exploiting multiple antennas to mitigate the adverse effects of fading and interference. Consequently, the OP diminishes further due to the improved resilience against signal degradation. However, an essential consideration arises due to the simultaneous presence of self-interference
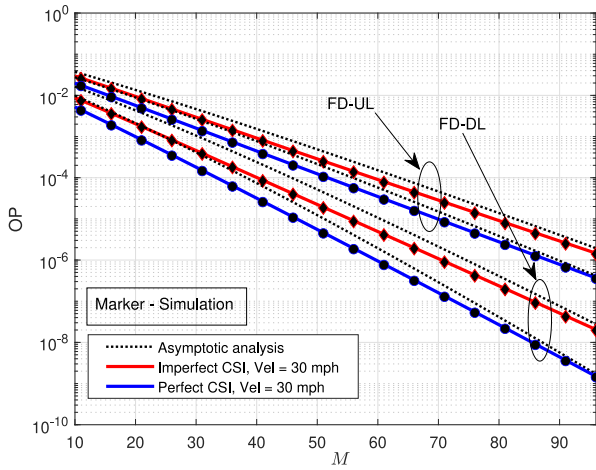
FIGURE 8. Asymptotic analysis of the OP of the proposed system for varying *M* under mobility case.

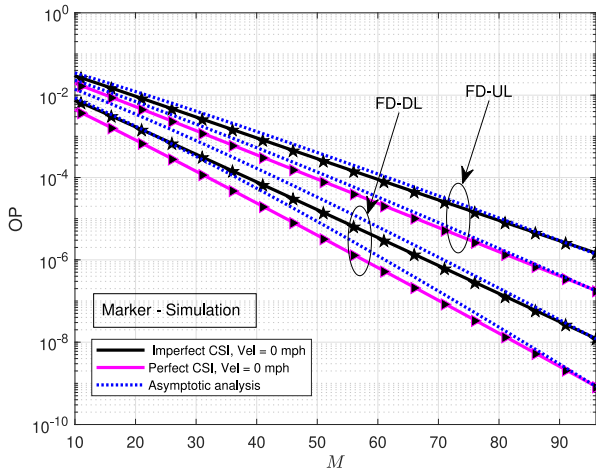**FIGURE 10.** Effect of FD and HD OP of the system for varying RI values.

FIGURE 9. Asymptotic analysis of the OP of the proposed system for varying *M* under immobility case.

(SI) in the UL and UDI in the DL. The introduction of SI in the UL and UDI in the DL has contrasting effects on the system's performance. Notably, the influence of SI in the UL is more pronounced than the impact of UDI in the DL. This asymmetry leads to a discernible reduction in the UL outage performance.

In Figs. 8 and 9, the trend in the OP for the devised system's mobility and immobility cases can be categorized into four distinct patterns, each of which can be elucidated as follows: 1) Increase in APs: The rise in the number of APs within the designated geographical area contributes to elevated SINR levels for all VCUs, resulting in improved communication conditions. Consequently, the system's outage performance experiences enhancement as more APs are available to cater to a larger number of VCUs. 2) Impact of Imperfect CSI: Comparing systems with perfect and imperfect CSI, the presence of imperfect CSI negatively affects the outage performance. Imperfect CSI leads to suboptimal resource allocation and signal processing, causing
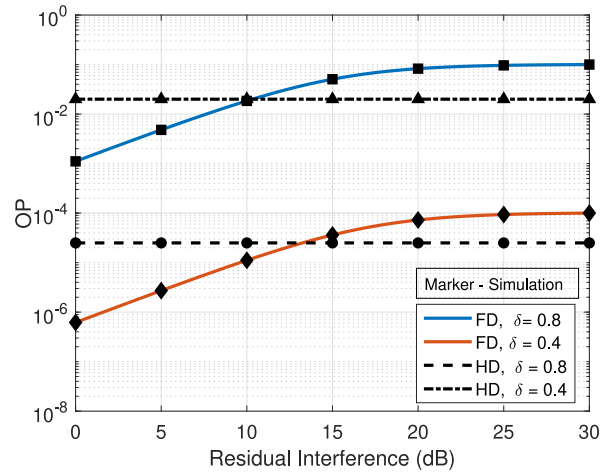
increased interference levels and reduced SINR. This, in turn, contributes to a degraded outage performance compared to scenarios where perfect CSI is assumed. 3) Asymptotic convergence: Notably, the convergence of asymptotic curves for a higher number of APs signifies the positive influence of enhanced diversity gain. The accumulation of multiple diverse signal paths due to increased APs enables improved signal reception, thereby mitigating the effects of fading and interference. This advantageous diversity gain reinforces the convergence of asymptotic curves, signifying better outage performance. 4) Effect of mobility: For immobile VCUs, the influence of time-selective fading becomes prominent. As the fading effect remains relatively constant over time due to limited mobility, the asymptotic curves converge more rapidly in the immobility case. This accelerated convergence reflects the consistent fading characteristics experienced by immobile VCUs, leading to quicker stabilization of communication conditions and convergence of outage probabilities.

Fig. 10 depicts the trend in the FD OP and HD OP for the devised system for varying RI values considering different shadow correlation values, i.e., $\delta = 0.8$ and $\delta = 0.4$. As RI increases, the FD OP also increases, indicating deteriorating system performance. The reason for this trend is due to fact that with higher RI, there is an increase in interference, which leads to more collisions and degradation in the quality of received signals in FD mode. This effect is particularly pronounced as the system tries to simultaneously transmit and receive on the same frequency band, causing self-interference to become more detrimental to signal detection and decoding. In contrast, there is no RI in the HD scheme, leading to constant performance across different RI values. Since HD mode alternates between transmission and reception, there is no concurrent transmission and reception occurring, thus eliminating the issue of self-interference. As a result, the system performance remains unaffected by changes in RI. For $\delta = 0.8$, HD mode consistently exhibits higher outage probabilities than FD mode when RI is less than 10 dB. This phenomenon can be explained by
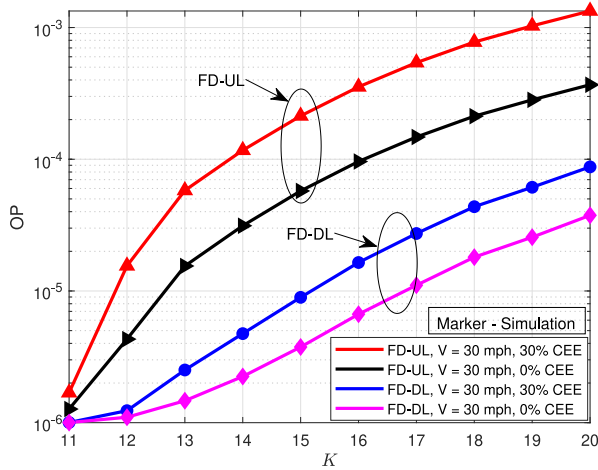
FIGURE 11. Effect of time-selective fading, CEE and pilot contamination.

considering the impact of channel correlation. In highly correlated channels (large δ), the interference in HD mode becomes more significant due to the constructive interference caused by correlated fading, resulting in higher outage probabilities compared to FD mode. Similarly, for $\delta = 0.4$, HD mode consistently shows higher outage probabilities than FD mode when RI is less than 13 dB. Again, the increased outage probabilities in HD mode can be attributed to the detrimental effects of correlated fading, which exacerbates interference and reduces the system's robustness against RI.

Fig. 11 depicts the impact of time-selective fading and CEE on the FD-UL OP and FD-DL OP of the proposed system for a fixed number of pilots (τ_p), i.e., 15. The figure presents a scenario where the velocity of VCUs is fixed at 30 mph, representing a moderate level of time-selective fading due to VCU mobility. This fading is characterized by variations in the channel's amplitude and phase caused by the Doppler effect. The analysis includes two levels of CEE: 0% and 30%. In the case of CEE = 0%, it is assumed that the MMSE channel estimation technique is employed, resulting in a highly accurate estimation of the actual channel conditions. The number of pilots is fixed at 15, which is insufficient to serve all VCUs uniquely, leading to pilot contamination. This contamination occurs when the same pilot signals are used by multiple VCUs, causing interference that degrades the quality of channel estimation. For both FD-UL and FD-DL, the figure likely shows an upward trend in OP with an increasing number of VCUs. This trend is more pronounced at 30% CEE compared to 0% CEE, indicating that higher estimation errors significantly affect system performance. The curves for FD-UL and FD-DL may differ slightly due to the inherent differences in uplink and downlink operations, such as power control and interference management. The analysis also highlights the compounded effect of time-selective fading and CEE on OP. With 30 mph VCU velocity, the time-selective fading introduces additional variability in the channel, which, when combined with CEE, results in a higher OP. This suggests that in environments with high mobility and significant CEEs, the system's ability to maintain reliable communication is severely challenged.

V. CONCLUSION

In this study, we explored the outage performance of a URLLC-enabled FD-CFm-MIMO system, integrating uniform quantization and realistic confined fronthaul links while accounting for VCU mobility and imperfect CSI scenarios. Leveraging the Welch-Satterthwaite approximation, we formulated a closed-form expression for OP and compared the system's results against its asymptotic outage metrics. Our analysis further encompassed the impact of imperfect CSI, pilot contamination, fronthaul quantization, and VCU mobility across diverse DPS models on the system's outage performance. Simulations underscored the system's bolstered outage performance with an augmented number of APs, antennas per AP, and a diminished number of VCUs. We observed that doubling the number of APs reduces FD-UL's OP by 50.617% and FD-DL's by 84.114%, improving URLLC reliability. Moreover, with VCUs in motion at a consistent speed of 30 mph and for $M = 120$, the Rectangular DPS model exhibits superior outage performance, with 1×10^{-9} lower probability compared to Uniform DPS and 8.9×10^{-8} lower probability compared to Gaussian DPS, attributed to its diverse fading characteristics. We also observed that the compounded effects of time-selective fading and CEE, particularly in high mobility scenarios, suggest a significant challenge in maintaining reliable communication. We compared the results of FD CFm-MIMO system with the benchmark HD CFm-MIMO system. It is observed that, at ($\delta = 0.8$), HD mode showed higher OP than FD mode for RI below 10 dB, while at ($\delta = 0.4$), HD mode's OP exceeds FD mode's for RI below 13 dB, underscoring the influence of channel correlation on system robustness. Moreover, our findings also revealed that the choice of moderate parameter values for $\tilde{a}$ and $\tilde{\sigma}_e^2$ (Case 3) is significant in enhancing the system performance.

REFERENCES

[1] K. Singh, F. Karim, S. K. Singh, P. K. Sharma, S. Mumtaz, and M. F. Flanagan, "Performance analysis of RIS-assisted full-duplex communications with infinite and finite blocklength codes," *IEEE Trans. Commun.*, vol. 71, no. 7, pp. 4262–4282, Jul. 2023.

[2] A. A. Nasir, H. D. Tuan, H. Q. Ngo, T. Q. Duong, and H. V. Poor, "Cell-free massive MIMO in the short blocklength regime for URLLC," *IEEE Trans. Wireless Commun.*, vol. 20, no. 9, pp. 5861–5871, Sep. 2021.

[3] B. Hazarika and K. Singh, "AFL-DMAAC: Integrated resource management and cooperative caching for URLLC-IoV networks," *IEEE Trans. Intell. Veh.*, early access, Aug. 10, 2023, doi: 10.1109/TIV.2023.3303932.

[4] S. Kurma, P. K. Sharma, K. Singh, S. Mumtaz, and C.-P. Li, "URLLC-based cooperative industrial IoT networks with nonlinear energy harvesting," *IEEE Trans. Ind. Informat.*, vol. 19, no. 2, pp. 2078–2088, Feb. 2023.

[5] Y. Lin, X. Na, D. Wang, X. Dai, and F.-Y. Wang, "Mobility 5.0: Smart logistics and transportation services in cyber-physical-social systems," *IEEE Trans. Intell. Veh.*, vol. 8, no. 6, pp. 3527–3532, Jun. 2023.

[6] J. Han, A. Sciarretta, L. L. Ojeda, G. De Nunzio, and L. Thibault, "Safe- and Eco-driving control for connected and automated electric vehicles using analytical state-constrained optimal solution," *IEEE Trans. Intell. Veh.*, vol. 3, no. 2, pp. 163–172, Jun. 2018.

[7] Y. Zhang et al., "The AD4CHE dataset and its application in typical congestion scenarios of traffic jam pilot systems," *IEEE Trans. Intell. Veh.*, vol. 8, no. 5, pp. 3312–3323, May 2023.

[8] H. Q. Ngo, A. Ashikhmin, H. Yang, E. G. Larsson, and T. L. Marzetta, "Cell-free massive MIMO versus small cells," *IEEE Trans. Wireless Commun.*, vol. 16, no. 3, pp. 1834–1850, Mar. 2017.

[9] S. Dhalbisoi, A. Rout, R. K. Sahoo, and S. Sethi, "A comparative analysis on 5G cell free massive MIMO in next generation networking environment," in *Proc. ICICCSP*, 2022, pp. 1–5.

[10] S. Kurma, P. K. Sharma, S. Dhok, K. Singh, and C.-P. Li, "Adaptive AF/DF two-way relaying in FD multi-user URLLC system with user mobility," *IEEE Trans. Wireless Commun.*, vol. 21, no. 12, pp. 10224–10241, Jun. 2022.

[11] P. Raut and P. K. Sharma, "Full-duplex multi-user pair scheduling with time-selective fading and imperfect CSI," in *Proc. NCC*, 2019, pp. 1–6.

[12] S. Kurma et al., "On the performance analysis of full-duplex cell-free massive MIMO with user mobility and imperfect CSI," TechRxiv, Preprint, 2022. [Online]. Available: https://www.techrxiv.org/articles/preprint/On_the_Performance_Analysis_of_Full-Duplex_Cell-Free_Massive_MIMO_with_User_Mobility_and_Imperfect_CSI/21685361/0

[13] B. Paden, M. Čáp, S. Z. Yong, D. Yershov, and E. Frazzoli, "A survey of motion planning and control techniques for self-driving urban vehicles," *IEEE Trans. Intell. Veh.*, vol. 1, no. 1, pp. 33–55, Mar. 2016.

[14] P. Saikia, S. Pala, K. Singh, S. K. Singh, and W.-J. Huang, "Proximal policy optimization for RIS-assisted full duplex 6G-V2X communications," *IEEE Trans. Intell. Veh.*, early access, May 12, 2023, doi: 10.1109/TIV.2023.3275632.

[15] T. T. Vu, D. T. Ngo, H. Q. Ngo, and T. Le-Ngoc, "Full-duplex cell-free massive MIMO," in *Proc. IEEE Int. Conf. Commun.*, 2019, pp. 1–6.

[16] S. Datta, D. N. Amudala, E. Sharma, R. Budhiraja, and S. S. Panwar, "Full-duplex cell-free massive MIMO systems: Analysis and decentralized optimization," *IEEE Open J. Commun. Soc.*, vol. 3, pp. 31–50, 2022.

[17] M. Bashar, K. Cumanan, A. G. Burr, H. Q. Ngo, M. Debbah, and P. Xiao, "Max–min rate of cell-free massive MIMO uplink with optimal uniform quantization," *IEEE Trans. Commun.*, vol. 67, no. 10, pp. 6796–6815, Oct. 2019.

[18] Y. Al-Eryani, M. Akrout, and E. Hossain, "Multiple access in cell-free networks: Outage performance, dynamic clustering, and deep reinforcement learning-based design," *IEEE J. Sel. Areas Commun.*, vol. 39, no. 4, pp. 1028–1042, Apr. 2021.

[19] S. Shekhar, M. Srinivasan, S. Kalyani, and M.-S. Alouini "Outage probability of uplink cell-free massive MIMO network with imperfect CSI using dimension-reduction method," 2023, *arXiv:2101.07737*.

[20] S. Kurma, K. Singh, P. K. Sharma, and C.-P. Li, "Outage probability analysis of uplink cell-free massive MIMO with user mobility," in *Proc. IEEE Mil. Commun. Conf.*, 2022, pp. 37–42.

[21] K. Ando, H. Iimori, T. Takahashi, K. Ishibashi, and G. T. F. De Abreu, "Uplink signal detection for scalable cell-free massive MIMO systems with robustness to rate-limited fronthaul," *IEEE Access*, vol. 9, pp. 102770–102782, 2021.

[22] Y. Xiao, P. Mähönen, and L. Simić, "Mobility performance analysis of scalable cell-free massive MIMO," 2022, *arXiv:2202.01488*.

[23] C. D'Andrea, G. Interdonato, and S. Buzzi, "User-centric handover in mmWave cell-free massive MIMO with user mobility," in *Proc. 29th Eur. Signal Process. Conf. (EUSIPCO)*, 2021, pp. 1–5.

[24] J. Zheng, J. Zhang, E. Björnson, Z. Li, and B. Ai, "Cell-free massive MIMO-OFDM for high-speed train communications," *IEEE J. Sel. Areas Commun.*, vol. 40, no. 10, pp. 2823–2839, Oct. 2022.

[25] D. Wang, M. Wang, P. Zhu, J. Li, J. Wang, and X. You, "Performance of network-assisted full-duplex for cell-free massive MIMO," *IEEE Trans. Commun.*, vol. 68, no. 3, pp. 1464–1478, Mar. 2020.

[26] H. V. Nguyen et al., "A novel heap-based pilot assignment for full duplex cell-free massive MIMO with zero-forcing," in *Proc. IEEE ICC*, 2020, pp. 1–6.

[27] B. Al-Nahhas, M. Obeed, A. Chaaban, and M. J. Hossain, "RIS-aided cell-free massive MIMO: Performance analysis and competitiveness," in *Proc. IEEE ICC*, 2021, pp. 1–6.

[28] A. Goldsmith, *Wireless Communications*. Cambridge, U.K.: Cambridge Univ. Press, 2005.

[29] E. Björnson and L. Sanguinetti, "Making cell-free massive MIMO competitive with MMSE processing and centralized implementation," *IEEE Trans. Wireless Commun.*, vol. 19, no. 1, pp. 77–90, Jan. 2020.

[30] C. Feng, Y. Jing, and S. Jin, "Interference and outage probability analysis for massive MIMO downlink with MF precoding," *IEEE Signal Process. Lett.*, vol. 23, no. 3, pp. 366–370, Mar. 2016.

[31] Q. Ding, H. Shi, and Y. Lian, "Outage probability and achievable rate analysis for massive MIMO downlink with mixed-DAC and MF precoding," *China Commun.*, vol. 17, no. 8, pp. 95–105, Aug. 2020.

[32] M. Abramowitz et al., *Handbook of Mathematical Functions with Formulas, Graphs, and Mathematical Tables*. New York, NY, USA: Dover, 1964.

[33] I. S. Gradshteyn and I. M. Ryzhik, *Table of Integrals, Series, and Products*, 7th ed., Amsterdam, The Netherlands: Elsevier, 2007.

[34] H. Cramer, "Random variables and probability distributions," in *Cambridge Tracts in Mathematics*. Cambridge, U.K.: Cambridge Univ. Press, 1970.

SRAVANI KURMA (Graduate Student Member, IEEE) received the B.Tech. degree in electronics and communication engineering from the JNTUH College of Engineering, Jagtial, India, in 2017, and the master's degree (Gold Medalist) in communication system engineering from the Visvesvaraya National Institute of Technology, Nagpur, India, in 2019. She is currently pursuing the Ph.D. degree with the Institute of Communications Engineering, National Sun Yat-sen University, Taiwan. Her current research interests include 5G, 6G, Industrial Internet of Things, wireless energy harvesting, cooperative communications, reconfigurable intelligent surfaces, full-duplex communication, cell-free MIMO, ultrareliable and low-latency communication, resource allocation, and machine learning for communication.

KESHAV SINGH (Member, IEEE) received the M.Sc. degree in information and telecommunications technologies from Athens Information Technology, Greece, in 2009, and the Ph.D. degree in communication engineering from National Central University, Taiwan, in 2015. He currently works with the Institute of Communications Engineering, National Sun Yat-sen University, Taiwan, as an Assistant Professor. From 2016 to 2019, he was a Research Associate with the Institute of Digital Communications, University of Edinburgh, U.K. From 2019 to 2020, he was a Research Fellow with University College Dublin, Ireland. He leads research in the areas of green communications, resource allocation, transceiver design for full-duplex radio, ultrareliable low-latency communication, nonorthogonal multiple access, machine learning for wireless communications, integrated sensing and communications, nonterrestrial networks, and large intelligent surface-assisted communications. He chaired workshops on conferences like IEEE GLOBECOM 2023 and IEEE WCNC 2024. He also serves as a Leading Guest Editor for IEEE TRANSACTIONS ON GREEN COMMUNICATIONS AND NETWORKING Special Issue on Design of Green Near-Field Wireless Communication Networks.

PRABHAT KUMAR SHARMA (Senior Member, IEEE) received the B.Tech. degree in electronics and communication engineering and VLSI design from Uttar Pradesh Technical University, Lucknow, the M.Tech. degree in electronics and communication engineering and VLSI design from the Malaviya National Institute of Technology, Jaipur, and the Ph.D. degree in wireless communications from the University of Delhi in 2015.

He is an Assistant Professor with the Department of Electronics and Communication Engineering, Visvesvaraya National Institute of Technology, Nagpur, India. He has authored over 80 journal and conference papers. His current research interests include physical-layer aspects of wireless, molecular and biological, and quantum communications. He is a recipient of the Visvesvaraya Young Faculty Research Fellowship from the Ministry of Electronics and Information Technology, Government of India. In 2019, He was awarded the URSI/InRaSS Young Indian Radio Scientist Award by the International Radio Science Union.

THEODOROS A. TSIFTSIS (Senior Member, IEEE) received the Ph.D. degree in electrical engineering from the University of Patras, Greece, in 2006.

He is a Professor with the Department of Informatics and Telecommunications, University of Thessaly, Greece. His research interests fall into the broad areas of communication theory and wireless communications with emphasis on wireless communications theory, reconfigurable intelligent surfaces, optical wireless communications, and physical-layer security.

Prof. Tsiftsis served on the editorial boards of the IEEE TRANSACTIONS ON COMMUNICATIONS, IEEE TRANSACTIONS ON VEHICULAR TECHNOLOGY, IEEE COMMUNICATIONS LETTERS, and IEEE TRANSACTIONS ON MOBILE COMPUTING. He is currently an Associate Editor of the IEEE TRANSACTIONS ON WIRELESS COMMUNICATIONS. He served as an IEEE Vehicular Technology Society Distinguished Lecturer from 2018 to 2022, and has recently appointed as an IEEE Communications Society Distinguished Lecturer from 2024 to 2025.

CHIH-PENG LI (Fellow, IEEE) received the B.S. degree in physics from National Tsing Hua University, Hsinchu, Taiwan, in June 1989, and the Ph.D. degree in electrical engineering from Cornell University, Ithaca, NY, USA, in December 1997.

From 1998 to 2000, he was a Technical Staff Member with Lucent Technologies. From 2001 to 2002, he was a Manager of Acer Mobile Networks. In 2002, he joined the faculty of the Institute of Communications Engineering, National Sun Yat-sen University (NSYSU), Taiwan, as an Assistant Professor. He has been promoted to a Full Professor in 2010. He served as the Chairman of the Department of Electrical Engineering, NSYSU from 2012 to 2015. He was the Director of the Joint Research and Development Center of NSYSU and Brogent Technologies from 2015 to 2016. He served as the Vice President of General Affairs with NSYSU from 2016 to 2017. He is currently the Dean of the Engineering College, NSYSU. His research interests include wireless communications, baseband signal processing, and data networks.

Dr. Li was the recipient of the 2014 Outstanding Electrical Engineering Professor Award of the Chinese Institute of Electrical Engineering Kaohsiung Section and the 2015 Outstanding Engineering Professor Award of the Chinese Institute of Engineers Kaohsiung Section. He is currently the Chair of the IEEE Broadcasting Technology Society Tainan Section. He also serves as an Editor for the IEEE TRANSACTIONS ON WIRELESS COMMUNICATIONS, an Associate Editor for the IEEE TRANSACTIONS ON BROADCASTING, the General Co-Chair for IEEE Information Theory Workshop 2017, and the Member of Board of Governors with IEEE Tainan Section. He was the Lead Guest Editor of the Special Issue of *International Journal of Antennas and Propagation*.